Functional Imaging-Based Diagnostic Strategy: Intra-axial Brain Masses

12

Arastoo Vossough and Seyed Ali Nabavizadeh

Introduction

Imaging plays an integral role in the management of brain tumors, including tumor diagnosis and classification, treatment planning, and post-treatment surveillance. Conventional magnetic resonance imaging (MRI) with gadolinium-based contrast agents on current high field clinical MR systems provides excellent anatomic and morphologic imaging of brain tumors. Anatomic MRI can determine the location of intracranial masses, presence of edema, mass effect, calcification, cyst formation, hemorrhage, vascularization, and contrast enhancement. Extra-axial and intra-axial brain tumors can also be discriminated quite accurately by anatomic imaging. However, the assessment of tumor type, grade, and extension, and differentiation of tumors from tumor-like conditions can be limited, potentially affecting therapeutic decision-making [1, 2].

Histopathological diagnosis, whether from stereotactic biopsy of masses or surgical resection, remains the reference standard for diagnosis and grading of brain tumors, in conjunction with newer genetic and molecular markers. However, there may be certain limitations. First, if the tissue is obtained by biopsy or incomplete resection, it only provides information about a portion of the neoplasm and not necessarily the entirety of the mass, resulting in potential sampling errors that may lead to inaccurate results, particularly in heterogenous tumors. Additionally, certain lesions cannot be treated surgically and may have a high risk for biopsy. Finally, there is significant variability even among experienced neuropathologists in the diagnosis of certain brain tumors [2].

A. Vossough (✉)
Department of Radiology, Children's Hospital of Philadelphia—University of Pennsylvania, Philadelphia, PA, USA
e-mail: vossough@email.chop.edu

S. A. Nabavizadeh
Department of Radiology, University of Pennsylvania, Philadelphia, PA, USA
e-mail: Seyedali.nabavizadeh@pennmedicine.upenn.edu

There are several advanced MRI techniques that have been used in the past two decades to assess various features of brain tumors. These include diffusion-weighted imaging (DWI), diffusion tensor imaging (DTI), perfusion imaging, and functional MRI (fMRI). These techniques have become more widespread secondary to emergence of higher magnetic field MR scanners, improved gradient systems, and greater availability of these acquisition and analysis methods. Integration of diagnostic information from various advanced MRI techniques can provide more reliable characterization of intra-axial brain masses, which are utilized in various aspects of brain management including tumor classification and grading, treatment planning, assessing response to treatment, and post-treatment surveillance [1, 3, 4].

In this chapter, first we will briefly review the applications of select advanced MRI techniques (diffusion-weighted imaging, MR spectroscopy, MR perfusion imaging) in brain tumor diagnosis. We will then present a multiparametric algorithmic approach for diagnosis of intra-axial brain masses, and finally conclude this chapter by discussing current challenges.

Magnetic Resonance Spectroscopy

Proton magnetic resonance spectroscopy (MRS) is a method that assays a number of chemically distinct proton species present in each voxel by detecting and capitalizing on slight differences in the chemical shift of different metabolites, and generates spectra reflecting their relative quantity in a sampled voxel of tissue. These differences in frequency are displayed on the x-axis of each spectrum in units of parts per million (ppm) of a standard reference compound, rather than in hertz, in order to make comparisons of different spectra taken in different magnetic fields feasible. The y-axis of the graph is often scaled relative to the highest peak, as direct quantification of metabolites is difficult in the clinical setting. MRS technique is adapted to record signals from metabolites present in tissues at much lower concentrations

S. H. Faro, F. B. Mohamed (eds.), *Functional Neuroradiology*, https://doi.org/10.1007/978-3-031-10909-6_12

compared to water, which provides the bulk of the signal in conventional MRI. Therefore, MRS depends on relatively small differences in signal-to-noise ratio and that is why high magnetic field systems have greatly improved MRS in recent years. Different acquisition methods can be used in proton MRS. Using long echo times (TE), the human brain clinical MRS spectrum is dominated by four major metabolites: (1) choline (3.2 ppm), (2) creatine (3.0 ppm), (3) *N*-acetyl aspartate (2 ppm), and (4) lactate (1.3 ppm). Short TE MRS enables us to define further metabolites with short T2 relaxation times such as myoinositol, lipids, amino acids, and macromolecules, some of which can be important in brain tumor imaging, as will be discussed later [5]. MRS has been used extensively to understand chemical pathology of brain tumors and surrounding tissues. Details of MR spectroscopy techniques are covered in other parts of this book. In this section, we briefly review different application of MRS in brain tumor imaging.

Metabolic Markers for Intra-axial Brain Tumors

Although numerous peaks are observed in an MRS spectrum, the most commonly useful peaks in evaluation of intra-axial brain tumors are choline (Cho), creatine (Cr), *N*-acetyl-aspartate (NAA), lactate and lipid (Lac, Lip), and myoinositol (mI) peaks [6]. The choline peak (3.2 ppm) is the sum of several compounds that are active in phospholipid metabolism (phosphatidylcholine, phosphoethanolamine, glycerophosphocholine, and glycerolphosphoethanolamine) [7]. It is generally considered a marker of membrane turnover (breakdown and proliferation) and is often increased in brain tumors. The total creatine (tCr) peak (3.02 ppm), which is composed of creatine and phosphocreatine, is a marker of metabolic activity. Traditionally, it has been considered a reference standard for relative quantification of other peaks based on the assumption that it is rather constant in a given tissue; however, studies of absolute tCr have partly challenged this old concept both in normal and tumoral tissues [8, 9]. Studies have shown decreased tCr in a subset of high-grade gliomas and elevation of tCrin low-grade gliomas and gliomatosis cerebri [8, 10, 11]. The *N*-acetyl aspartate (NAA) peak (2 ppm) is generally considered to be a neuronal marker. It is found to be decreased in most brain tumors [11]. Due to difficulties in separation of lactate (Lac, 1.31 ppm), and lipid (Lip, 1.33 ppm) peaks, especially at short TE, they are often reported as a combined Lactate + Lipid peak. Separation of lactate is possible by using intermediate or long TE values, which results in J-coupling of the 1.3 ppm lactate peak with its partner at 4.1 ppm resulting in an inverted peak. Presence of lactate has traditionally been considered to be an indicator of alteration in glucose metabolism, with increased glycolysis in poorly oxygenated portions of brain tumors. It is most often seen in high-grade gliomas and metastases; although it is also seen in some cases of grade II gliomas [11]. Elevation of lipid (Lip) peaks (0.9 ppm and 1.3 ppm) are also a feature of high-grade glioma and metastasis, but is often not seen in low-grade tumors [8, 11]. Lipids are generally better defined at short TE due to their short T2 relaxation time. Myoinositol (mI) peak (3.56 ppm) is generally considered a glial marker. Due to rapid transverse relaxation, it is only observed on short TE spectroscopy. Different investigators have shown high mI in low-grade gliomas and decrease in mI as glioma grade increases [10, 12].

More recently, mutations in the genes isocitrate dehydrogenase 1 and 2 (IDH1 and IDH2) have been shown in large percentages of grade II and grade III gliomas and secondary glioblastomas [13, 14]. These are key enzymes in cellular metabolism, epigenetic regulation, DNA repair, and redox states. These mutations cause abnormally high levels of D-2-hydroxyglutarate (2HG) in tumor tissue and are associated with improved responses to tumors. Relevant inhibitors are also being investigated as targets for brain tumor treatments. This increased level may be detected in vivo by more advanced spectral-edited magnetic spectroscopy, and be used for characterization of glial neoplasms. A recent meta-analysis demonstrated excellent sensitivity and specificity of 2HG MRS for prediction of IDH mutant gliomas [15].

Differential Diagnosis, Preoperative Tumor Grading, and Biopsy Guidance

The role of MRS in differential diagnosis of intra-axial brain masses largely depends on comparison with conventional and other advanced imaging features, as MRS is rarely specific enough to support a net diagnosis by itself. One of these roles is assisting in differentiation of brain abscesses from rim-enhancing brain tumors and tumor cysts, which reportedly can be made by the detection of amino acid (0.9 ppm), alanine (1.5 ppm), acetate (1.9 ppm), and succinate (2.4 ppm) peaks in abscesses [16]. In contrast, the presence of elevated choline in the cystic component of a rim-enhancing mass is more in favor of a tumoral cyst [17]. Some infracts can also mimic tumors in some stages of their evolution. MRS may support the diagnosis of ischemia, by showing elevated lactate peak in the context of absence or decrease of other metabolites [18], but the diagnosis becomes more challenging if choline elevation is encountered due to rapid cell membrane breakdown, making this application of MRS less useful clinically [17, 19, 20]. Differentiation of active demyelination from brain tumor can be very difficult as both can show contrast enhancement and choline can be elevated in both, due to active membrane destruction/turnover in the former and active membrane proliferation in the latter. NAA can also be depressed in both entities, due to neuronal injury

in both entities and neoplastic tumor cell in the case of tumors [17–20]. Therefore, other advanced imaging methods such as perfusion imaging can be more helpful in differentiation of some forms of active demyelination from brain tumors [4]. MRS has also been used for differentiation between low-grade gliomas and focal cortical developmental malformations by showing more increase of Cho and decrease of NAA in low-grade gliomas than in focal cortical developmental malformations, though elevated choline may not be detected in a minority of low-grade gliomas [21, 22].

Some studies have been performed to investigate the added diagnostic value of MRS, compared to conventional imaging alone in evaluation of brain masses. In one large study, Moller-Hartmann et al. investigated 176 consecutive patients with different brain masses and concluded that addition of MRS significantly increased the proportion of correctly diagnosed cases from 55% to 71% [23]. In addition, there were no cases where a correct diagnosis on MRI was mistakenly discarded due to the MRS findings. In another study, Ando et al. reported that the addition of MRS information to contrast-enhanced MRI findings increased diagnostic sensitivity without altering specificity [24].

During the past decades, there has been an effort to find specific MRS tumor markers for different brain neoplasms. By and large, these studies have revealed a gross correlation between Cho/NAA and Cho/Cr peak height ratios and glioma grade [21, 25, 26]. Similarly, the presence of elevated lipid/lactate suggests the presence of a high-grade tumor [25]. The generally encountered limitation for using MRS in preoperative tumor grading has been significant overlap between high- and low-grade tumors [27], therefore different threshold values have been proposed to improve the accuracy of MRS in tumor grading [1]. Kim et al. showed that both short and intermediate TEs are useful in differentiating high-grade from low-grade gliomas. In this study, the main difference between the spectra with different TEs was that, at short TE, Cho/Cr and Cho/NAA ratios were significantly lower compared to the intermediate TE spectra. This is due to the T2 relaxation time of choline, which is longer than those of Cr and NAA [28]. Although use of short TE MRS can give information about metabolites that are not evident on intermediate and long TE, it has been shown that at short TE, a significant percentage of low-grade tumors may show lack of choline elevation and near-normal Cho/Cr ratios, causing diagnostic confusion in some patients [29]. A few studies have compared the ability of MRS in tumor grading with other advanced imaging techniques and suggested that MR perfusion imaging is more accurate than MRS in tumor grading [1, 30]. The same concepts related to tumor grading can be utilized in biopsy guidance and MRS has been shown to increase the accuracy of stereotactic biopsies by targeting areas with high Cho/NAA ratios in a heterogeneous glial neoplasm [31, 32]. Targeting biopsy to regions with highest lipid content has also been suggested to be helpful in improving the diagnostic yield of biopsy [33]. In a similar fashion, MRS has also been used to guide stereotactic radiosurgery to areas with higher Cho/NAA ratios [34, 35].

Another area of MRS research in the field of brain tumor imaging is differentiation between high-grade gliomas and single metastases. Some studies have focused on comparison of the spectra from the enhancing parts of the tumors with emphasis on different lipid ratios [36, 37], while other studies have evaluated the peritumoral regions [38, 39]. In the literature, the "peritumoral region" often refers to the areas surrounding the enhancing portions of tumor (peri-enhancement region). Overall, it seems that evaluation of the peritumoral region is more helpful in differentiation of high-grade gliomas from solitary metastases by showing increased choline or choline ratios in high-grade tumors, but not in metastasis [38–40]. It is thought that the peritumoral region in primary high-grade gliomas contains infiltrating neoplastic cells, hence altering the choline ratios, whereas the peritumoral region in a typical metastasis is mostly edema without substantial tumor cell infiltration, and therefore has a more normal appearing MRS spectrum. In one study, the peritumoral region demonstrated the most significant differences in metabolite ratios [41]. The Cho/Cr ratio in glioblastomas was significantly higher than that in metastases. Additionally, elevated Cho/Cr levels were also noted in lymphomas compared to metastases, and lymphoma showed higher lipids+lactate/Cr levels compared with glioblastomas and metastases.

Determination of the extent of brain tumors has also been studied using MR spectroscopy. Generally, tumor extent has been investigated based on Cho/NAA ratios in the peritumoral region. For more accurate measurements, an index known as Choline-NAA index (CNI) has been proposed, where CNI is the number of standard deviations between the Cho-to-NAA ratio within a given voxel and that of the control voxels [42]. One of these studies correlated MRS data with histopathologic findings of stereotactic biopsy and showed that a CNI of greater than 2.5 has a high sensitivity and specificity for predicting the presence of tumor in the biopsy sample [43]. Using the Cho-NAA index concept, studies have shown that three-dimensional (3D) MRS can significantly alter radiation therapy target volumes [44, 45]. With more widespread availability of advanced combined neuronavigation technology and intraoperative MRI, MRS may potentially have a stronger therapeutic impact in the future by better defining the true extent of brain tumors during surgery [46].

Use of MRS in order to predict progression in low-grade brain tumors has been addressed in a few studies with conflicting results. Some of these studies have reported that increased choline signal and decreased Cho/NAA ratio may be used to detect early dedifferentiation of low-grade glial

tumors [47–49]. However, others did not find MRS to be useful for this purpose [50]. In terms of prognostic value of MRS, a study in low-grade gliomas revealed that elevated tCr was associated with worse outcome compared to those with normal or reduced tCr [51]. Another study of glioblastomas demonstrated that patients with a high volume of elevated CNI have a less favorable prognosis [52]. Finally, a relatively recent concept has been to measure whole-brain NAA in order to assess global burden of a brain tumor. The idea behind this concept is that high-grade gliomas are infiltrative, but their visible degree of infiltration by current conventional and advanced techniques is an underestimation of actual burden. One study has shown a decrease in whole-brain NAA in patients with high-grade glioma, with this decrease being approximately 30% more than expected by the visible tumor burden [53]. The actual clinical significance of this measurement, particularly with respect to prognosis prediction, remains to be fully determined.

Therapeutic Monitoring

Evaluation of tumor response to radiotherapy and chemotherapy with conventional imaging may take a long time to be reliably detected. Another very important limitation of anatomical imaging is in the evaluation of treatment response in low-grade gliomas, which are typically slow growing and non-enhancing. Application of physiologic imaging techniques such as MRS may potentially be helpful in distinguishing true tumor recurrence/progression from treatment-related changes. Several studies have evaluated the role of MRS to assess treatment response. Decreased choline levels and concomitant increase in Lip+Lac has been found as a marker of response to radiotherapy in some studies [54–56]. Similar changes have also been described as early markers of treatment following chemotherapy in high-grade gliomas [57, 58]. Serial spectroscopic monitoring of treatment response to chemotherapy has also been evaluated in low-grade gliomas and a decreased choline level has been reported, suggesting a potential role for MRS in these types of tumors [59].

One of the other limitations of conventional imaging in brain tumors is distinction between radiation necrosis and recurrence following treatment. Several studies have reported that MRS can be useful to differentiate these two entities by showing increased Chol/Cr or Cho/NAA ratio over time in recurrent tumor, and have therefore concluded that serial MRS may differentiate these two entities with reasonable accuracy [24, 60–63]. However, in real clinical settings there are at least two problems. The first problem is that radiation necrosis and recurrent tumor often coexist together in the same region, with different proportions. The other problem, which is inherent to all serial MRS studies, is that spatial variation in metabolite sampling within an individual tumor can be much greater than the change in these peaks over time if there are slight differences in voxel placement between two scans or patient motion. Similarly, any change in acquisition technique can make the assessment of longitudinal change unreliable. Therefore, it is very likely that these parameters cannot be as optimally controlled in actual clinical settings compared to research studies with a small number of selected patients where each MRS study was closely controlled by a highly trained spectroscopist or neuroradiologist.

Diffusion Imaging

Diffusion-weighted imaging (DWI) is a technique that is sensitive to Brownian motion of tissue water. Although DWI has emerged as a technique for early detection of acute cerebral ischemia, it has been increasingly used in other disorders of the central nervous system (CNS). DWI has been used extensively in different aspects of brain tumor imaging including diagnosis, treatment planning, and therapeutic monitoring. Detailed technical aspects of DWI are beyond the scope of this chapter and will be covered in other chapters; however, in summary, diffusion sequences are made by adding an additional pair of gradient pulses to render an MR signal, which is sensitive to the mobility of water molecules. Any molecular movement between first and second pulses results in incomplete rephrasing of the signal, which can lead to signal loss. In addition to diffusion rate of water molecules, DWI signal intensity also includes a T2-weighted component. Therefore, true reduced diffusion is estimated and measured by comparing diffusion-weighted (trace) images, with the same image acquisitions without diffusion weighting (b-zero) on a voxel by voxel basis, which results in generation of an "apparent diffusion coefficient" (ADC) or diffusivity map. Use of higher numbers of diffusion gradient directions, multiple diffusion strengths (B levels), and non-Gaussian assessment of diffusion has also led to additional diffusion-derived techniques such as diffusion tensor imaging, high angular resolution diffusion imaging (HARDI), diffusion kurtosis imaging (DKI), and others. These techniques allow additional diffusion-derived parameters to be assessed such as fractional anisotropy, axial diffusivity, radial diffusivity, track density, and various indices of kurtosis. Many of these parameters have not yet found their way into routine clinical practice at this time.

Differential Diagnosis, Preoperative Tumor Grading, and Biopsy Guidance

DWI in conjunction with conventional MRI has been proved to be useful in differential diagnosis of intra-axial brain lesions. Quantitative ADC maps have been useful in trying to differentiate tumors from abscesses, demyelinating plaques, and radiation-induced necrosis [64–67]. The viscous and cellular pus in abscesses produce a low ADC that in many cases can distinguish these lesions from facilitated diffusion in necrotic tumor. Low ADC has also been noted as a typical feature of radiation necrosis, while demyelinating plaques typically have normal or facilitated diffusion, although some may have more peripheral areas of restricted diffusion [68]. Another useful application of DWI in brain tumor imaging is assessment of cellularity. A low ADC in an intra-axial neoplasm can often be seen in lymphoma or metastasis secondary to relative increased cellularity and decreased tissue water. This finding has been noted to be helpful in differentiating these lesions from many gliomas, which show generally higher ADC values, but it should be mentioned that decreased diffusivity can be detected in cellular high-grade gliomas as well [69, 70]. A few reports have been published in which a direct comparison of ADC values with the Ki-67 index was performed, and most found a significant inverse correlation between ADC values and Ki-67 [71, 72].

Another area of potential application of DWI has been in preoperative grading of gliomas. Several studies have found an inverse correlation between areas of minimum ADC (ADC_{min}) within the tumor and glioma grade, and different cutoff values have been proposed [73], but significant overlap between high and low grade exists in most of these studies [25, 74]. A study claimed that using a combination of minimum ADC and ADC difference values (which is the difference between minimum and maximum ADC) facilitates the preoperative grading of astrocytic tumors [75]. Despite these efforts, multiparametric studies showed that using ADC alone is less useful than combined studies with MR spectroscopy and MR perfusion in grading of gliomas [30]. Other studies have shown that histogram analysis of ADC values is useful in distinguishing low-grade astrocytomas and oligodendrogliomas [76], and another study in oligodendrogliomas found a relationship between the 1p/19q codeletion genotype and ADC values [77]. There has been recent interest in use of high b-value DWI in preoperative grading of glioma. DWI with a high *b* value (generally in the range of 3000–4000 s/mm^2 rather than the more typical 1000 s/mm^2) allows the characteristics of water diffusion to be studied in more detail [78]. The rationale for using these techniques is that diffusing water molecules can be divided into two pools, one of which diffuses at a faster rate than the other. Alvarez-Linera et al. investigated 54 patients with gliomas and compared ADC with *b* values of 1000 and 3000 s/mm^2. They observed that most of the patients with high- and low-grade gliomas showed areas of increased signal intensity on images obtained with a b value of 1000 s/mm^2. However, with a b value of 3000 s/mm^2, the areas of increased signal intensity were seen in most patients with high-grade gliomas, while most of the low-grade gliomas showed no area of increased signal intensity [79]. Another study by Seo et al. also concluded that DWI at $b = 3000$ s/mm^2 is more useful than DWI at $b = 1000$ s/mm^2 in terms of discriminating high-grade and low-grade gliomas at 3 T [80]. The exact role of high b-value DWI in grading of gliomas remains to be determined in prospective studies, especially in comparison with MR spectroscopy and MR perfusion imaging.

Another observation that has been encountered in high-grade gliomas is variability in ADC_{min}, even in tumors of the same grade and histology [81, 82]. Although part of this may be explained by presence of necrosis and hemorrhage, which is very common in these types of tumors, it may also be indicative of heterogeneity of cellularity among tumors of the same grade and it seems to be a confounding factor in preoperative prediction of histological grade. Reports have also suggested that ADC_{min} may be useful in prediction of radiation responsiveness in high-grade gliomas [82]. In cases of highly heterogeneous tumor, attention to the ADC map before biopsy and sampling the area of minimum ADC has been shown to improve the diagnostic yield of biopsy, and better correlation with histology [83]. In one study, an inverse correlation was found between relative ADC and various histopathologic features of aggressiveness [84]. Newer techniques such as diffusion tensor imaging (DTI) and diffusion kurtosis imaging (DKI) have also been applied in the grading of brain tumors, mostly in a research setting. One meta-analysis showed that high-grade gliomas had decreased average mean diffusivity values compared with low-grade gliomas in the tumor core and increased average mean diffusivity values in the peripheral region [85]. High-grade gliomas had increased FA values compared with low-grade gliomas in the tumor core, decreased values in the peripheral region, and a decreased fractional anisotropy difference between the tumor core and peripheral region. A meta-analysis of ten studies reported that DKI metrics had an accuracy a sensitivity of 0.85 and specificity of 0.92 for distinguishing low-grade and high-grade gliomas [86].

Application of DWI for delineation of tumor margins has been addressed in some studies. Generally, these studies have not correlated the location of DWI abnormality with histopathology, and instead they compared DWI parameters of peritumoral edema in high-grade tumors with other tumors, based on the presumption that high-grade glioma cells infiltrate surrounding brain, but other tumors (metastases, meningioma) do not. Some of these studies have shown higher ADC values in the peritumoral edema for metastases compared to high-grade gliomas [38, 87]. On the other hand,

some studies have concluded that DWI cannot reliably differentiate edema with infiltration of tumor cells from pure vasogenic edema [88, 89]. There is only one study that directly correlated ADC in specific locations with histopathologic examination findings of neuroimaging-navigated biopsy specimens, and it showed considerable overlap between the ADC of tumor and peritumoral tissues, failing to provide important additional diagnostic information [90]. A meta-analysis of nine studies with DTI concluded that high-grade gliomas may be distinguished from brain metastases by comparing the peritumoral FA and MD values but not by intralesional DTI metrics [91]. Diffusion imaging using high *b* values may potentially be able to better differentiate tumor tissue from peritumoral edema by demonstrating specific diffusion abnormalities in the evaluation of edema surrounding a mass. However, this remains speculative and requires further studies with histopathologic correlation.

Therapeutic Monitoring and Prognostication

Currently, the imaging standard by which response to treatment is determined is change in enhancing tumor size in sequential MRI examinations [92]. However, these changes in tumor size may take many months to become apparent. There has been a research trend to use DWI to measure the response of brain tumors after therapy. The rationale for using DWI is that treatment of a tumor with cytotoxic agents may result in significant cell death, which in turn will reduce the total cellularity and this can be detected as a change in ADC values. Results of a few studies have revealed that serial measurements of ADC at early time points following treatment may be able to assess dynamic response to treatment, and differentiate responsive from non-responsive tumors [93, 94]. Low ADC after chemoradiation therapy has been shown to be a poor prognostic marker [95]. Diffusion imaging has also shown to be useful as a predictor of response in patients with brain metastases treated by stereotactic radiosurgery [96].

A few studies have evaluated the role of DWI in differentiation of radiation necrosis from recurrent tumor and have demonstrated restricted diffusion in some patients with radiation necrosis [65, 67]. One study that combined DWI and MR spectroscopy revealed that DWI does not provide additional information to MR spectroscopy in differentiation of radiation necrosis and recurrent tumor [97]. Al Sayyari A et al. [98] in a retrospective study of 17 patients revealed that susceptibility-weighted MRI-guided apparent diffusion coefficient analysis is helpful in differentiation of recurrent tumor from radiation injury. Determination of the actual added value of DWI in the diagnosis of this entity warrants further studies.

The final issue is the role of DWI in predicting patient prognosis. Two prospective studies have shown that preoperative ADC measurements in high-grade gliomas can predict patient prognosis [72, 99]. Another study has shown that ADC measurements within contrast enhancing regions of primary central nervous system lymphoma tumors is predictive of the patients' clinical outcome, both in terms of progression-free and overall survival [100]. Ellingson et al. reported application of diffusion analysis in a patient with gliomatosis cerebri, which correlated well with progressive decline in neurological status despite no change in traditional magnetic resonance images [101]. A study of 34 patients with low-grade glioma revealed that the ADC parameters were not a useful predictor of malignant transformation [102]. In phase II clinical trials of antiangiogenic agents for recurrent glioblastoma, baseline ADC was found to be a marker for overall survival in these patients [103]. One recent study did not find added prognostic value of diffusion kurtosis imaging measures in patients with glioblastoma [104]. Utility of more recent advanced diffusion techniques needs to be validated in larger studies.

Perfusion Magnetic Resonance Imaging

In the brain MRI literature, perfusion MRI refers to an all-encompassing term of various methods to measure hemodynamically derived functional parameters. Perfusion MRI can be done without contrast injection by tagging intravascular protons using various MR labeling schemes (arterial spin labeling) or can be performed via two general approaches using dynamic gadolinium-based contrast injection. The first approach is termed dynamic contrast-enhanced (DCE) MRI and is based on relaxivity measurements using a steady-state T1-weighted sequence during gadolinium contrast administration over a period of several minutes. The second approach is termed dynamic susceptibility contrast (DSC) MRI and is based on susceptibility effects using T2- or more commonly T2*-weighted images acquired over approximately 1–3 min, during which a high concentration bolus of gadolinium chelate rapidly passes through the brain. DSC perfusion imaging is the most commonly studied and clinically used technique in assessment of brain masses and will be discussed in this section. This method was initially described approximately three decades ago and is based on the principle that the signal change that occurs during passage of a high concentration bolus of gadolinium contrast in the vessels causes a difference in susceptibility between the contrast-containing vessels and brain tissue, and that this signal change can be converted to a relaxation rate change proportional to the fraction of blood volume within each voxel [105, 106]. These relative blood volume measurements are used to construct a relative cerebral blood volume (rCBV) map [107].

There are multiple technical considerations in the use of DSC imaging in the assessment of brain tumors. Accuracy of rCBV maps can vary substantially depending on the acquisition and postprocessing methods [108]. First is the choice of imaging sequence. In order to increase temporal resolution during dynamic contrast administration, currently most centers use an echo planar imaging (EPI)-based method. Different investigators have used spin echo EPI, gradient echo EPI, or a combination of both [109–111]. It is important to take into consideration the type of acquisition in applying research results for characterization of brain tumors, as the results and thresholds may vary [112]. Spin echo methods are sensitive to smaller vessels and capillaries, whereas gradient echo methods are sensitive to both small and large vessel perfusion [109, 112]. Using spin echo sequences may be helpful near the skull base or at bone or air interfaces, as they are less susceptible to artifacts. Most centers currently use gradient echo sequences for performing clinical DSC perfusion MRI in the assessment of brain tumors. This technique is very sensitive to structures that cause magnetic field inhomogeneity such as blood, calcium, bone, metals, or near air interfaces such as at the skull base. Reducing slice thickness and parallel imaging can be used to decrease these effects, but if larger coverage is needed, the interslice gap could be increased [113].

Another issue in the use of DSC perfusion imaging in tumor assessment is contrast leakage within brain tumors, which can lead to underestimation and inaccuracy of rCBV measurements, and potentially affect clinical interpretation. One way to solve this problem is to use correction algorithms to compensate and correct for leakiness in these tumors. It has been shown that corrected rCBV maps correlated with glioma tumor grade while uncorrected maps did not [114]. Another approach is to employ a dual-echo gradient echo acquisition [108], but this is not widely used. Finally one solution is to administer a small preload dose of contrast prior to performing the DSC perfusion MRI bolus injection to allow for leakage [108]. This preload injection can serve a dual purpose and be used for performing DCE imaging in the same MRI session as well.

Simultaneous GRE and SE DSC acquisition allows the potential calculation of vessel size index from the ratio of GRE to SE relaxivity without additional scan time and also obviate the need for preload injection; however, these techniques are not yet standardized [110, 115, 116].

In addition to the established processing techniques, described in previous section, there are additional techniques that can be used to process DSC data. Independent component analysis (ICA) is a technique that applies a data-driven, multivariate approach to categorize voxel time series and it has been mainly used to analyze functional MRI (fMRI) data by examining voxels exhibiting the same temporal response patterns [117]. LaViolette et al. used ICA to classify voxels with perfusion characteristics of both arteries and veins in patients with de novo GBM and patients with recurrent high-grade glioma before and after bevacizumab treatment. They demonstrated that arterio-venous overlap (AVOL) volume was significantly greater than the percentage of AVOL in nontumor vasculature. They also demonstrated that patients with decrease in AVOL after treatment showed an increase in overall survival, while rCBV and enhancing volume measures did not significantly differ across groups [118].

Another utilized technique is principal component analysis (PCA) which is a standard dimensionality reduction method [119]. In this type of analysis, the first principal component captures the highest amount of variance, with each succeeding components have the highest variance. Recently, Akbari et al. used PCA to analyze the peritumoral region in patients with glioblastoma using different aspects of DSC MRI time series such as baseline signal, depth and slope of signal decrease, signal recovery, and percentage of signal recovery. Their study demonstrated that PCA shows near-perfect accuracy in separating highly infiltrated tissues from regions that were unlikely to be infiltrated with tumor. They also created a heterogeneity map that predicted subsequent recurrence [119].

DCE perfusion MRI can be analyzed using two general approaches. The first and simpler approach is model-free analysis of the area under the time–signal intensity curve (AUC) during a given time. The advantage of this technique is that it is easier to perform without the need for complex postprocessing models. The second way to analyze DCE data is to use a pharmacokinetic model to quantify different metrics. The most commonly used model is the modified Tofts model. Each voxel in the Tofts model can contain three components: tissue parenchymal cells, blood vessels, and the tissue extracellular extravascular space (EES). The main parameters calculated by this model are Ktrans which is a measure of microvascular permeability, total plasma space volume (Vp), total extravascular-extracellular space volume (Ve), and Kep which is the reflux rate of gadolinium from the EES back into plasma [120].

The baseline T1 value would be needed to obtain concentration-time curve pharmacokinetic parameters in DCE imaging [121]. There are generally two approaches for establishing the T1 value. An estimate of baseline T1 value can be derived by using different techniques such as multiple flip angles or inversion recovery techniques [122, 123]. The downside of this approach is that estimation of the baseline T1 would be sensitive to noise from multiple factors such as scale factor miscalibration and motion [121, 124]. Another approach would be to use a fixed baseline T1 value based on available literature. The latter approach can generate more consistent results and can save several minutes of scanner time over the first method. The downside of using a fixed T1 value is that since it is not physiologic to the patient, some of

the calculated Ve values may be more than 100%, which is not possible [125]. A recent study published by Nam et al. demonstrated that Ktrans calculated from the fixed T1 acted as a preferable marker to differentiate true progression from pseudoprogression in patients with glioblastoma [123]. Another study by Tietze et al. demonstrated that although a fixed T1 introduced a bias into the DCE calculation, it did not have a major effect on the accuracy for differentiating high-grade from low-grade gliomas [121].

Arterial spin labeling (ASL) is an increasingly used imaging technique for measuring perfusion by using water molecules in blood vessels without the need for exogenous contrast material. This technique provides a potential advantage over DSC and DCE perfusion techniques given the increasing concern with gadolinium deposition in the brain. There are multiple different approaches for ASL image acquisition, but in general baseline control images are acquired through the area of interest followed by reimaging the area of interest after tagging the blood within the vessels in a slab of tissue proximally which would typically be the upper neck in brain ASL. Final images will be generated by subtracting the tagged from the control images in order to tease out the exchange rate of tagged water molecules with the static tissue as a representation of blood flow [126, 127]. Most current clinical scanners have an ASL sequence available as a commercial sequence option and PASL (Pulsed Arterial Spin Labeling) and pCASL (pseudo-Continuous Arterial Spin Labeling) are considered the most commonly used sequences. CASL (Continuous Arterial Spin Labeling), which was the first developed ASL sequence, is now considered obsolete given the difficult implementation and significant tissue energy deposition [126, 127].

Role of Perfusion Imaging in Preoperative Tumor Grading and Biopsy Guidance

Dynamic susceptibility contrast (DSC) perfusion MRI has been extensively studied in brain tumors [1, 128–131]. Several studies have demonstrated that CBV measurements have clinical value in grading of cerebral gliomas. Typically, the CBV value derived from DSC is not fully quantitative and often calculated as a ratio to the contralateral normal appearing white matter, providing relative CBV (rCBV) values. Maximum rCBV values of low-grade gliomas has been reported between 1.11 and 2.14, whereas maximum rCBV of high-grade gliomas were between 3.54 and 7.32 [1, 113, 128, 132, 133]. In one study, using an rCBV threshold of 1.5 provided a 100% sensitivity for detecting high-grade gliomas. In a larger study, using the rCBV threshold of 1.75 provided a sensitivity of 95% and specificity of 57.5% in differentiation of high-grade and low-grade gliomas. Some low-grade gliomas can have high CBV and therefore confound this accuracy, particularly oligodendrogliomas which will be discussed later in the chapter [134–136]. Perfusion MRI has also been used in distinguishing high-grade gliomas from lymphomas, which could have a similar appearance on conventional MRI, demonstrating that lymphomas have lower mean rCBV values. Nevertheless, in that study the presence of a very leaky blood brain barrier may have contributed to lower-than-expected rCBV measurements [137]. Perfusion imaging has also been used to differentiate high-grade gliomas from solitary metastases [38, 39]. The peritumoral rCBV is shown to be higher in primary high-grade gliomas than in metastases, due to the infiltrative nature of high-grade gliomas beyond the enhancing margin.

DCE imaging has also been studies for glioma grading. Jia et al. showed that Ktrans and Ve were significantly lower in low-grade gliomas compared to high-grade gliomas, with cutoff values of 0.035 min^{-1} and 0.13, respectively [138]. Jung et al. demonstrated that histogram analysis of Ktrans, Ve, and Vp obtained from the entire-tumor volume data were useful for grading gliomas; however, the 98th percentile Ktrans was the only variable to independently differentiate high- and low-grade gliomas [125]. In addition, Mills et al. demonstrated that high values of Ktrans were associated with the presence of frank necrosis and high values of Ve were associated with a fibrillary histologic pattern and with increased mitotic activity [139].

A number of studies have demonstrated that ASL imaging can have utility in adult glioma grading [140, 141] and also can predict histopathologic vascular density [141]. In a recent study comparing DSC and ASL imaging, Arisawa et al. demonstrated a strong correlations in the 75th percentile, mean, median, and standard deviation values between the ASL and DSC images; however, the area under the curve values was greater for the DSC images comparing ASL images indicating superiority of DSC imaging in glioma grading [142]. A recent meta-analysis of ASL in differentiating low- and high-grade glioma reported a sensitivity of 085–0.88 and specificity of 0.80 and 0.83, depending on the type of ASL technique [143].

Perfusion MRI has also been used in guiding stereotactic biopsy and radiosurgery in glioma patients. Traditionally, T1-weighted postcontrast MR sequences have been used to direct stereotactic biopsy targeting of enhancing masses, and fluid-attenuated inversion recovery (FLAIR) or T2-weighted sequences for non-enhancing masses. The rationale for using perfusion data is based on the utility in defining the most hypervascular region of the tumor [113, 144]. The region of highest vascularity and presumably highest malignancy does not necessarily correspond to the areas of contrast enhancement (contrast leakage) or there may be varying degrees of perfusion within the contrast enhancing portions of the tumor.

Therapeutic Monitoring and Prognostication

It is thought that at least half of low-grade astrocytomas will eventually dedifferentiate into high-grade tumors over the years. It has been shown that DSC MR may show increases in rCBV up to 12 months before the development of contrast enhancement in low-grade gliomas, potentially contributing to prediction of malignant transformation [145]. Law and colleagues have also retrospectively compared the value of rCBV measurements in predicting patient outcome in low- and high-grade gliomas [146]. They demonstrated that rCBV was an independent predictor of time to progression and clinical outcome. Using an rCBV threshold of 1.75 (compared to contralateral white matter) they were able to predict median time to progression in patients with gliomas, regardless of whether the tumor was low grade or high grade on pathology. Choi et al. demonstrated that higher Ktrans and Ve are associated with worse prognosis in patients with glioblastoma [147]. In a study of 24 patients with glioma using ASL imaging, Furtner et al. demonstrated that using maximum tumor blood flow cutoff value of 182 mL/100 g/min, patients with low-perfused gliomas had significantly longer event-free survival compared to patients with high-perfused gliomas independent of the WHO glioma grade [148]. A recent study comparing DSC vs ASL in 69 subjects with WHO Grade 3–4 gliomas demonstrated that rCBV measurements derived from DSC imaging provide the best sensitivity and specificity to predict tumor recurrence and survival time [149].

DSC perfusion imaging has been used in multiple studies as a predictive response marker of different treatment agents, most commonly antiangiogenic agents [150–152]. Baseline rCBV has been shown to correlate with overall survival in patients with high grade glioma receiving bevacizumab treatment [150, 152]. Another study in patients with recurrent GBM demonstrated that baseline rCBV stratified progression-free survival and overall survival in bevacizumab-treated patients. This study showed that a rCBV above the cutoff value of 3.92 was associated with halving of the median survival in comparison to rCBV below the cutoff, suggesting that rCBV may be a predictive biomarker in GBM patients in the setting of bevacizumab treatment [151].

DSC perfusion imaging has also been used as an early response biomarker in patients with high grade glioma in the setting of chemoradiation and antiangiogenic treatment. In a study of 36 patients with GBM who were treated with radiation and temozolomide, the percentage change in rCBV at 1 month after chemoradiation correlated with overall survival. Furthermore, increased rCBV after treatment was a strong predictor of poor survival. The study also showed a greater area under the ROC curves for 1-year survival assessed by rCBV than by tumor size [153]. Galban et al. used parametric response mapping (PRM) which is a voxel-wise approach for image analysis. They used rCBV and rCBF maps before treatment and after 1 and 3 weeks of therapy in 44 patients with high grade glioma and showed that the percentage change of rCBV or rCBF based on standard ROI placement did not predict survival, whereas the regional response evaluations made on the basis of PRM were highly predictive of survival [154]. The results of this study were corroborated in a subsequent study that compared three different methodologies including percentage change of whole tumor statistics (i.e., mean, median, and percentiles), the physiological tumor segmentation (low rCBV, medium rCBV, or high rCBV), and PRM in 44 patients with high grade glioma that were imaged pre-therapy and 1 and 3 weeks after initiation of chemoradiation. They demonstrated that PRM was the only analytical approach found to generate a response metric significantly predictive of patient 1-year survival [155].

A multi-center study of DSC perfusion MRI in patients with recurrent GBM receiving bevacizumab combined with irinotecan or temozolomide demonstrated that patients surviving at least 1 year had significantly larger decreases in rCBV at week 2 and 16 of treatment and patients with increased rCBV from baseline had significantly shorter OS than those with decreased rCBV at both week 2 and week 16 [156]. In a recent meta-analysis, Choi et al. evaluated the value of DSc and DCE perfusion MRI as a predictive/prognostic biomarker in patients with recurrent glioma treated with a bevacizumab-based regimen. Based on analysis of 13 studies, they demonstrated that the pooled hazard ratios between responders and non-responders as determined by rCBV were 0.46 for progression-free survival based on analysis of 226 patients and 0.47 for overall survival based on analysis of 247 patients. This indicates that rCBV is helpful for predicting disease progression and also eventual outcome after treatment [157]. They also demonstrated that most perfusion and permeability MRI parameters (rCBV, Ktrans, CBVmax, Vp, Ve, and Kep) demonstrated a consistent decrease on the follow-up MRI after treatment [157].

Intra-axial Brain Mass Diagnostic Strategy

Traditionally, the first step in the characterization of intracranial masses is determination of whether the mass is intra-axial or extra-axial. Extra-axial masses may arise from bone, cartilage, meninges, vasculature, cranial nerves, or be metastatic. Conventional high-resolution MRI is often accurate in distinguishing intra-axial from extra-axial masses. While conventional MRI is useful for the characterization of intra-axial brain masses, there are significant areas of diagnostic overlap and limitations for the accurate classification of

brain neoplasms and masses. Use of diagnostic information from advanced MRI techniques has potential to further improve the classification accuracy of conventional anatomic imaging [3, 4].

Imaging experts and researchers in the field of brain tumor imaging have been utilizing added information from advanced MRI for a long time. However, in the clinical arena, integration of all the various advanced MRI techniques (diffusion-weighted imaging, perfusion-weighted imaging, MR spectroscopy) into a relatively well-defined and easy-to-follow diagnostic strategy or algorithm would be desirable for the physician interpreting the imaging of brain masses. An example of such diagnostic algorithmic approach, from the authors' own institution, in combining conventional and advanced MRI for characterization of intra-axial brain masses in adults is shown in Fig. 12.1 [3, 4]. It is important to recognize that any such diagnostic strategy or algorithm be considered in conjunction with the conventional MRI features and appearances of brain masses, the patients' clinical context, and the information from other imaging modalities such as computed tomography and nuclear medicine. Additionally, it is important to realize that any such algorithm is imperfect and will have diagnostic pitfalls and exceptions, and the advanced imaging data that feeds into this algorithm may have technical and postprocessing nuances that should be understood and duly considered for optimal interpretation and management. In particular, parameter cutoff numerical values should not be viewed as definitive perfect delimiters given some degree of inherent variability in determining these types of thresholds.

In order to better understand and utilize algorithmic approaches to advanced imaging in brain masses, we will first briefly summarize the typical advanced MRI features of various intra-axial brain masses [3, 4, 83, 158–160]. Again note that the following descriptions are the typical findings in each category and are present in the majority of cases, but there will always be exceptions to the typical imaging features and presentations of these lesions.

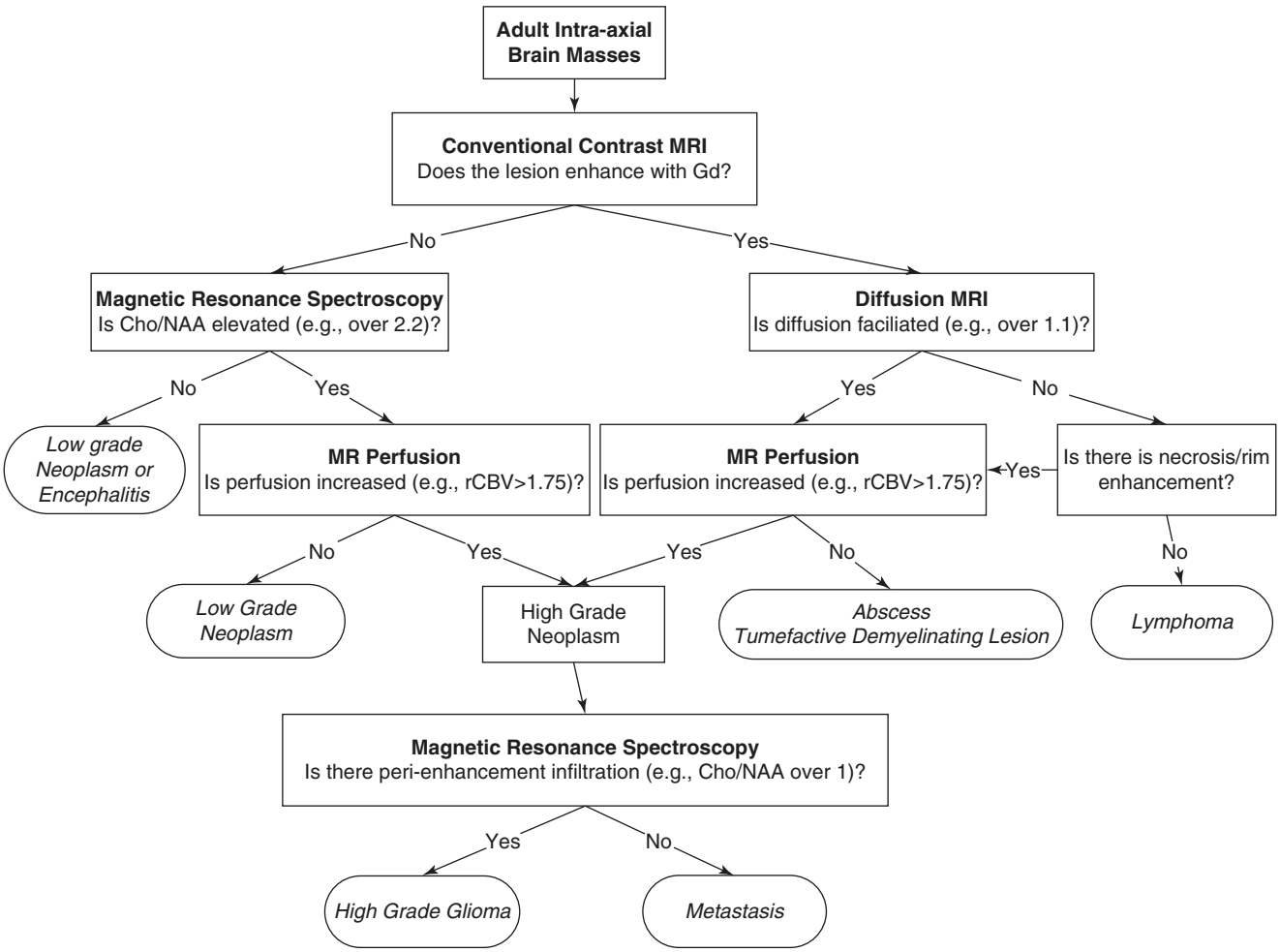

Fig. 12.1 An example of a diagnostic algorithm to assist in classification of unknown intra-axial brain masses. This algorithm combines conventional MRI features (enhancement) with advanced MRI features of brain masses (diffusion, perfusion, spectroscopy). (Adapted from [3, 4]. Please note that the thresholds noted in these algorithms are informative and not definitive)

High-Grade Gliomas

High-grade gliomas typically enhance with contrast, mostly in a heterogeneous fashion, and may have nonenhancing areas of necrosis. Diffusion imaging findings are variable and often the ADC is heterogeneous within these masses, but highly cellular tumors (for example some solid portions of glioblastomas) may have reduced diffusion. On MR spectroscopy, there is typically elevated choline (sometimes markedly), decreased NAA, and increased lipid+lactate levels (especially in glioblastoma). There is no perfect spectroscopic cutoff value to differentiate high-grade and low-grade gliomas, but a choline/NAA cutoff ratio of 2.2 has been suggested to separate high-grade versus low-grade glioma and non-neoplastic conditions [3]. On DWI, the signal characteristics of high-grade tumors is dependent on tumor cellularity [69]. Since different tumors may have different cellularity or even different parts of the same tumor may have various degrees of cellularity, the ADC values are variable. Glioblastomas often have hypercellular regions and are therefore more likely to have areas of reduced diffusion [69, 161]. MR perfusion imaging typically demonstrates elevated blood volume (often greater than 1.75 compared to contralateral white matter) [1]. An example of advanced imaging features a high-grade glioma is shown in Fig. 12.2. There is considerable variability in the appearance of glioblastoma as defined more recently using molecular and genetic criteria.

Low-Grade Gliomas

Low grade diffuse fibrillary astrocytomas typically do not enhance with contrast material. Other low-grade primary neoplasms such as pilocytic astrocytomas, mixed neuronal glial cell tumors, and low-grade oligodendrogliomas may demonstrate contrast enhancement. Diffusion imaging findings are again variable and there is overlap between high- and low-grade tumors, though generally the ADC value of low-grade tumors is higher than high-grade gliomas [83]. On MR spectroscopy, low-grade gliomas often, but not always,

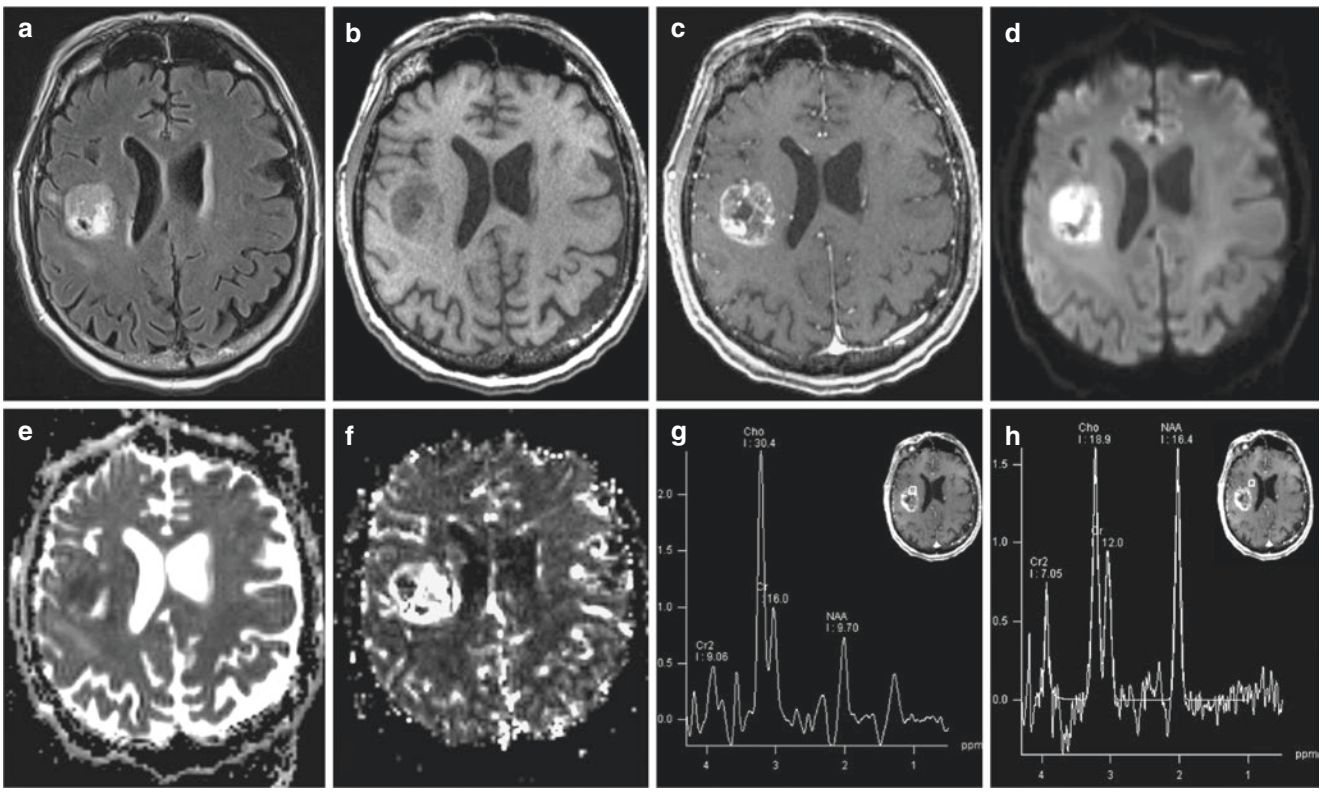

Fig. 12.2 Conventional and advanced MRI in primary high-grade glial neoplasm (glioblastoma). (**a**) Axial FLAIR image demonstrates a mass in the right cerebral hemisphere, with heterogeneous signal. (**b**) Axial precontrast T1-weighted image shows heterogeneous hypointensity within the lesion. (**c**) Postcontrast T1-weighted image shows heterogeneous contrast enhancement within the mass. (**d**) DWI image shows high signal intensity, which on the ADC map (**e**) is confirmed to be reduced diffusion in the bulk of the mass, and T2 shine-through along the posteromedial aspect of the mass. (**f**) CBV map derived from dynamic susceptibility contrast perfusion imaging demonstrates markedly elevated blood volume in large portions of the mass compared to the contralateral white matter. (**g**) MRS spectrum from a voxel placed over the enhancing portion of the mass demonstrates markedly elevated Cho/Cr and Cho/NAA ratios. (**h**) MRI spectrum from a voxel placed outside the enhancing portion of the mass demonstrates elevated Cho/Cr ratio and slightly elevated Cho/NAA ratio, suggesting that there is infiltrating neoplasm beyond the enhancing margins of the mass, therefore suggesting that it is an infiltrating primary high-grade tumor

have elevated choline and variable decrease in NAA. The degree of choline elevation is generally less than in high-grade gliomas, but there is overlap between the two. Myoinositol is elevated in many low-grade gliomas. On perfusion MRI, most low-grade gliomas, especially fibrillary astrocytomas do not have elevated rCBV, though again oligodendrogliomas and some pilocytic astrocytomas could have elevated rCBV despite being low-grade. An example of a low-grade glioma is shown in Fig. 12.3.

Primary Central Nervous System Lymphoma

In immunocompetent patients, lymphomas typically present with single or multiple, often homogeneous enhancing lesions that may mimic high-grade gliomas on conventional MRI. On MR spectroscopy, they typically have increased choline, reduced NAA, and increased lipid+lactate. In immunosuppressed patients, lymphoma may have peripheral or rim enhancement rather than solid enhancement. In AIDS

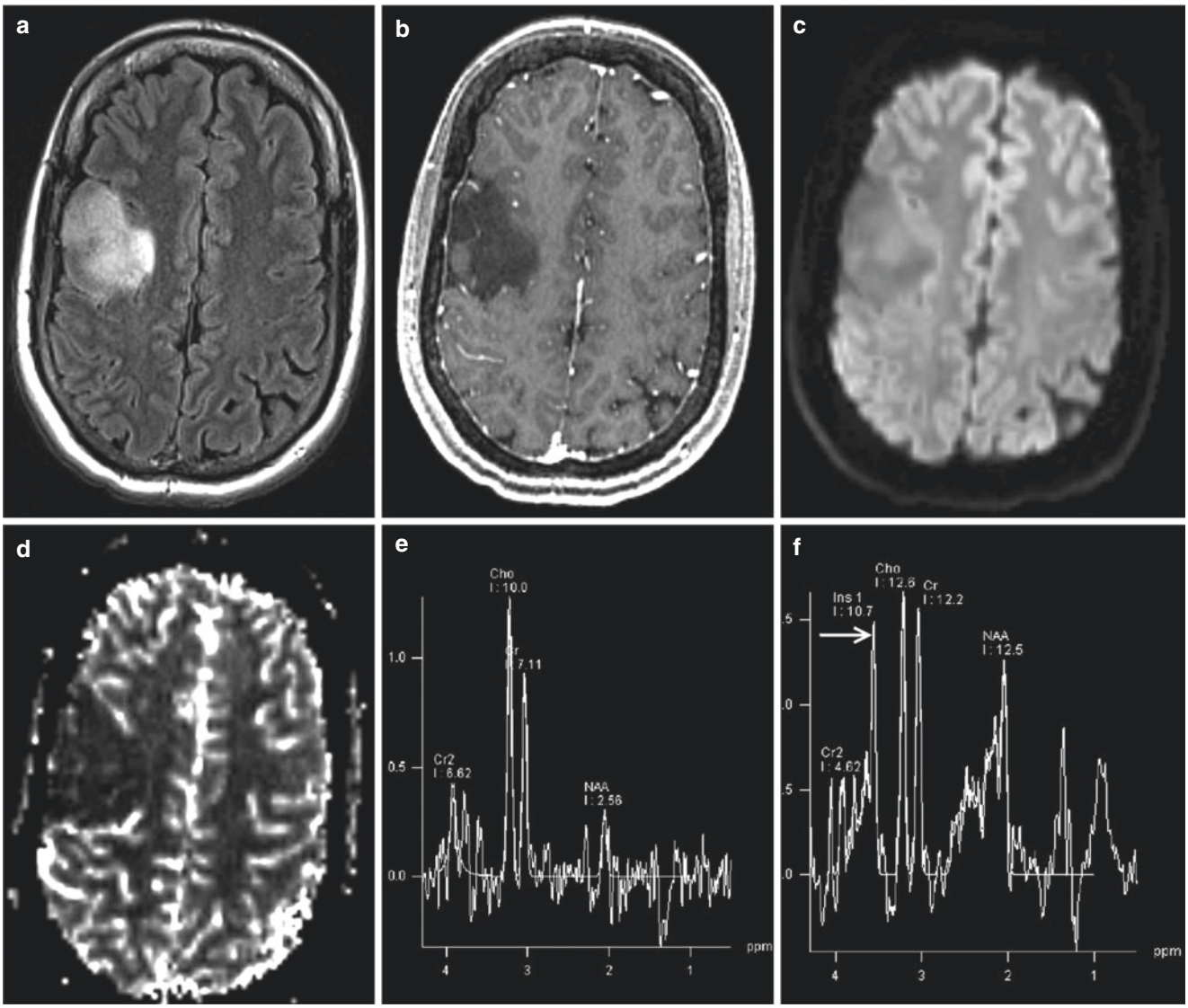

Fig. 12.3 Conventional and advanced MRI in a patient with a grade II astrocytoma. (**a**) Axial FLAIR image demonstrates a hyperintense mass in the right frontal lobe. (**b**) Postcontrast T1-weighted images demonstrate no contrast enhancement. (**c**) DWI image shows no restricted diffusion within the mass lesion. (**d**) CBV map derived from dynamic susceptibility contrast perfusion imaging demonstrates low blood volume within the mass. (**e**) MRS performed with TE = 135 ms on the mass lesion demonstrates elevated Cho/Cr and Cho/NAA ratios. (**f**) MRS performed with a short TE = 30 ms on the mass lesion demonstrates high myoinositol level at 3.56 ppm (arrow)

patients, toxoplasmosis can have elevated lipid and lactate, but often other metabolites are very low to absent on MR spectroscopy [162]. On diffusion-weighted imaging, lymphomas classically have reduced diffusion secondary to high cellularity and increased nucleus to cytoplasm ratio [69]. On perfusion imaging, lymphomas typically have low blood volume compared to high-grade gliomas and metastases, though the CBV of lymphomas could be variable. The CBV of lymphomas is typically higher than that of toxoplasmosis [163]. The enhancement of lymphomas is thought to be due to blood brain barrier destruction and not due to neovascularization [130]. Analysis of time intensity curve of DSC perfusion images has been reported to help in differentiating lymphoma from glioblastoma and metastasis. In lymphoma, percentage signal return is typically higher compared to glioblastoma and metastasis and can even show an overshoot over the baseline signal intensity, which is reflective of a T1 effect secondary to contrast extravasation [164, 165].

In a multiparametric study comparing 28 patients with glioblastoma of atypical appearance (solid enhancement with no visible necrosis) with 19 patients with lymphoma, Kickingereder et al. demonstrated that ADC and rCBV values were significantly lower in patients with PCNSL compared to glioblastoma. In addition, presence of intratumoral susceptibility signal (ITSS) was significantly lower in patients with PCNSL [166]. They also showed that combined multiparametric assessment of mean ADC, mean rCBV, and presence of ITSS significantly improved the differentiating PCNSL and atypical glioblastoma when compared to evaluation of one or two imaging parameters [166]. In a recent study of 42 patients with GBM and 18 patients with PCNSL who underwent conventional MRI, diffusion-weighted imaging, and DCE-MRI before surgery, PCNSLs demonstrated significantly lower rADC, but higher Ktrans and Ve compared to GBMs. The combination of rADC and Ktrans significantly improved the diagnostic ability for discriminating between PCNSL and GBM with area under the ROC curve = 0.930 [167]. An example of a primary CNS lymphoma in an immunocompetent patient is shown in Fig. 12.4.

Brain Metastases

Brain metastases can have a variable imaging appearance, depending on the underlying neoplasm, stage of disease, and patient's treatment status. The majority of brain metastases demonstrate enhancement, which could be solid, patchy, or peripheral. Solitary metastases may mimic primary brain tumors, especially high-grade gliomas. High-grade gliomas are infiltrative and often there is significant tumor infiltration beyond the enhancing part of the tumor, whereas the area surrounding the enhancing portion of the brain metastasis is thought to typically just represent edema. On MR spectroscopy, features of metastases are similar to high-grade neoplasms and include elevated choline and lipid+lactate, and reduced or absent NAA. Some studies have suggested that there is higher lipid within metastatic lesions [23, 168], but this is of limited use in clinical MR spectroscopy. On the other hand, spectroscopic interrogation of the areas around the enhancing portion of the mass has been shown to be more promising [39, 169]. In one study, a Cho/NAA cutoff ratio of 1 was shown to have excellent accuracy in differentiating the two [169]. On diffusion imaging, the ADC values of metastases are variable and partly dependent on the primary tumor. Many metastases have an elevated ADC, but certain types of tumors, especially hypercellular lesions such as small cell lung cancer metastases, may demonstrate reduced diffusion [170]. Peritumoral diffusion imaging also has shown higher ADC values in metastases compared to primary neoplasms [87]. Similarly on perfusion imaging, there is often elevated blood volume in the enhancing portion of metastases as there is in high-grade primary gliomas; however, there is higher peritumoral blood volume in infiltrative primary neoplasms compared to metastatic lesions [39, 130].

Cha et al. reported that analysis of time intensity curve of DSC perfusion images can differentiate single brain metastasis from glioblastoma. They demonstrated that the percentage of signal intensity recovery is reduced in both enhancing and peritumoral T2 prolongation in patients with metastasis compared to glioblastoma [171]. An example of a typical brain metastasis is shown in Fig. 12.5.

Tumefactive Demyelinating Lesions

Tumefactive demyelinating lesions are uncommon, but can mimic brain tumors, and given the marked difference in management, accurate diagnosis of these lesions is important in order to prevent unnecessary surgery as much as feasible. On MR spectroscopy, these lesions demonstrate a nonspecific elevation of choline and sometimes reduced NAA, which is not very helpful in distinguishing these lesions from neoplastic etiologies [172, 173]. Diffusion-weighted imaging is variable. ADC is often elevated, but sometimes acute demyelinating foci could have reduced diffusion. On perfusion imaging, tumefactive demyelinating lesions typically have low blood volume measurements, lower than high-grade gliomas and metastases and sometimes lower than normal brain tissue [130, 174]. An example of the typical tumefactive demyelinating lesion is shown in Fig. 12.6.

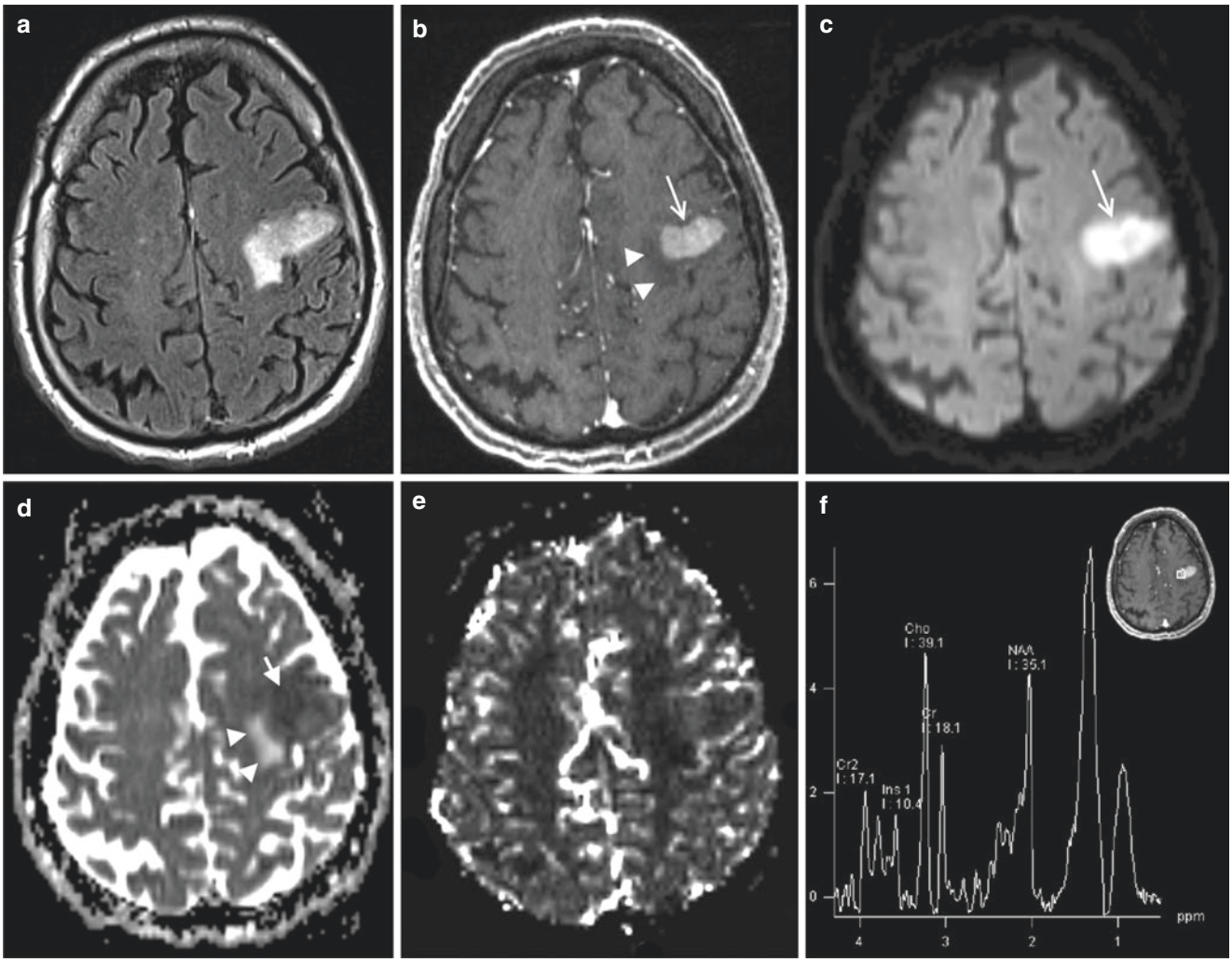

Fig. 12.4 Conventional and advanced MRI in a 72-year-old patient with primary central nervous system lymphoma. The patient was not immunosuppressed. (**a**) Axial FLAIR image shows a hyperintense mass lesion in the left frontal lobe. (**b**) Postcontrast T1-weighted image demonstrates rather homogeneous enhancement in the mass lesion (arrow) with an area of T1 hypointensity along the medial aspect of the mass (arrowheads). (**c**) Diffusion-weighted imaging shows high signal in the enhancing portion of the mass (arrow), confirmed to be reduced diffusion (arrow) on the ADC map (**d**). There is an area of facilitated diffusion in keeping with vasogenic edema along the medial aspect of the mass (arrowheads). (**e**) CBV map from dynamic susceptibility contrast perfusion imaging demonstrates only slight elevated blood volume in a portion of the enhancing mass lesion compared to the contralateral white matter (ratio less than 1.75). (**f**) MRS spectrum through the mass shows some elevation of Cho/Cr and Cho/NAA ratios

Encephalitis

The imaging features of encephalitides are highly variable among different etiologies that cause encephalitis. On MR spectroscopy, it has been reported that they have nonspecific elevation of choline and myoinositol, reduced NAA, with or without elevated lactate. The MRS spectrum is often similar to those of low-grade gliomas [3, 175]. On diffusion imaging, the ADC values of encephalitides are quite variable, and depends on the etiology and stage of disease. Acute encephalitis may frequently have restricted diffusion. Perfusion characteristics of encephalitides have not been well defined in the literature. Anecdotal experience and reports suggest that it is variable [3, 176, 177].

Brain Abscesses

The imaging features of brain abscesses may also be variable depending on etiology (bacterial, fungal), location, and the patient's immune status. MR spectroscopy demonstrates increased lactate, amino acids, alanine, acetate, succinate,

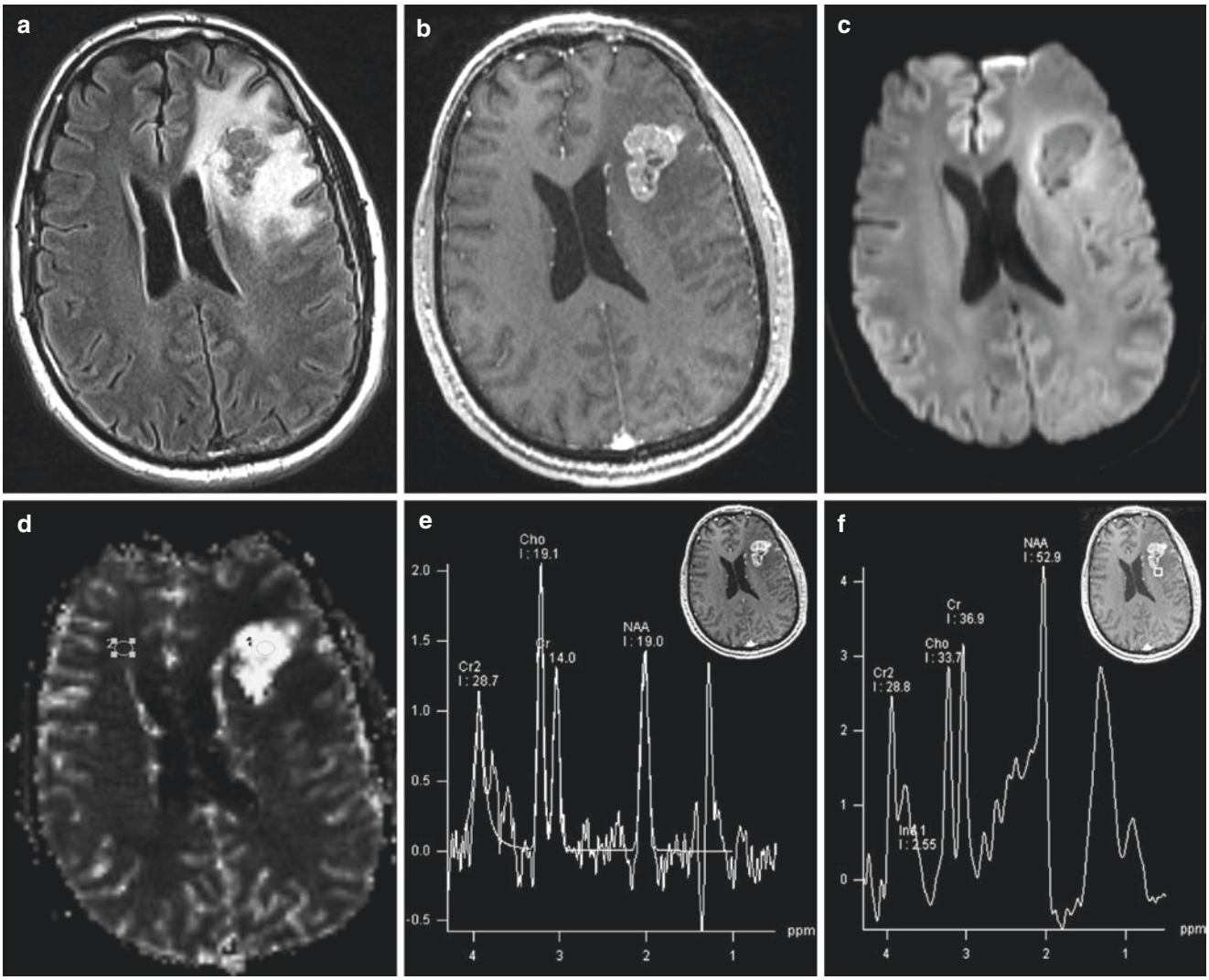

Fig. 12.5 Conventional and advanced MRI in a patient with brain metastases, subsequently found to have undifferentiated carcinoma of the colon. (**a**) Axial FLAIR image demonstrates an irregular mass in the left frontal lobe with surrounding vasogenic edema. (**b**) The lesion demonstrates heterogeneous, but mostly avid contrast enhancement on postcontrast T1-weighted images. (**c**) DWI image demonstrates that the lesion itself is relatively isointense to white matter (metastases can have variable diffusion characteristics based on type of tumor). (**d**) CBV map from dynamic susceptibility contrast perfusion imaging demonstrates markedly elevated blood volume in the mass lesion compared to the contralateral white matter (see regions of interest placement). The CBV ratio between the mass and contralateral white matter in this particular case was greater than 8. There is no increased blood volume in the areas surrounding the enhancing portion of the mass. (**e**) MRS spectrum from a voxel placed over the enhancing portion of the mass demonstrates elevated Cho/Cr and Cho/NAA ratios. (**f**) MRI spectrum from a voxel placed close to, but outside the enhancing portion of the mass demonstrates normal Cho/Cr and Cho/NAA ratios, suggesting that this is likely a metastatic lesion without substantial infiltrating neoplastic tissue beyond the enhancing portions of the mass

and lack of the normal brain tissue metabolites NAA, creatine, and choline within the abscess [178, 179]. On diffusion imaging, the central necrotic portion of processes often has markedly reduced ADC. The cystic portions of tumors often have facilitated diffusion, but occasionally, some brain tumors, especially those with hemorrhage, may show central restricted diffusion. A meta-analysis of 11 studies showed that diffusion imaging can differentiate brain abscess from other ring-enhancing lesions (not just tumors) with pooled sensitivity and specificity of 0.95 and 0.94, respectively [180]. On perfusion imaging, obviously the centrally necrotic portion of abscesses will have no or very low blood volume. The walls of abscesses typically have lower CBV measurements compared to high CBV in high-grade gliomas [3, 181]. It should be kept in mind, however, that some infectious lesions such as fungal infections and tuberculomas can have elevated rCBV values because of reactive neovascularization; but rCBV is still typically less than that for HGGs

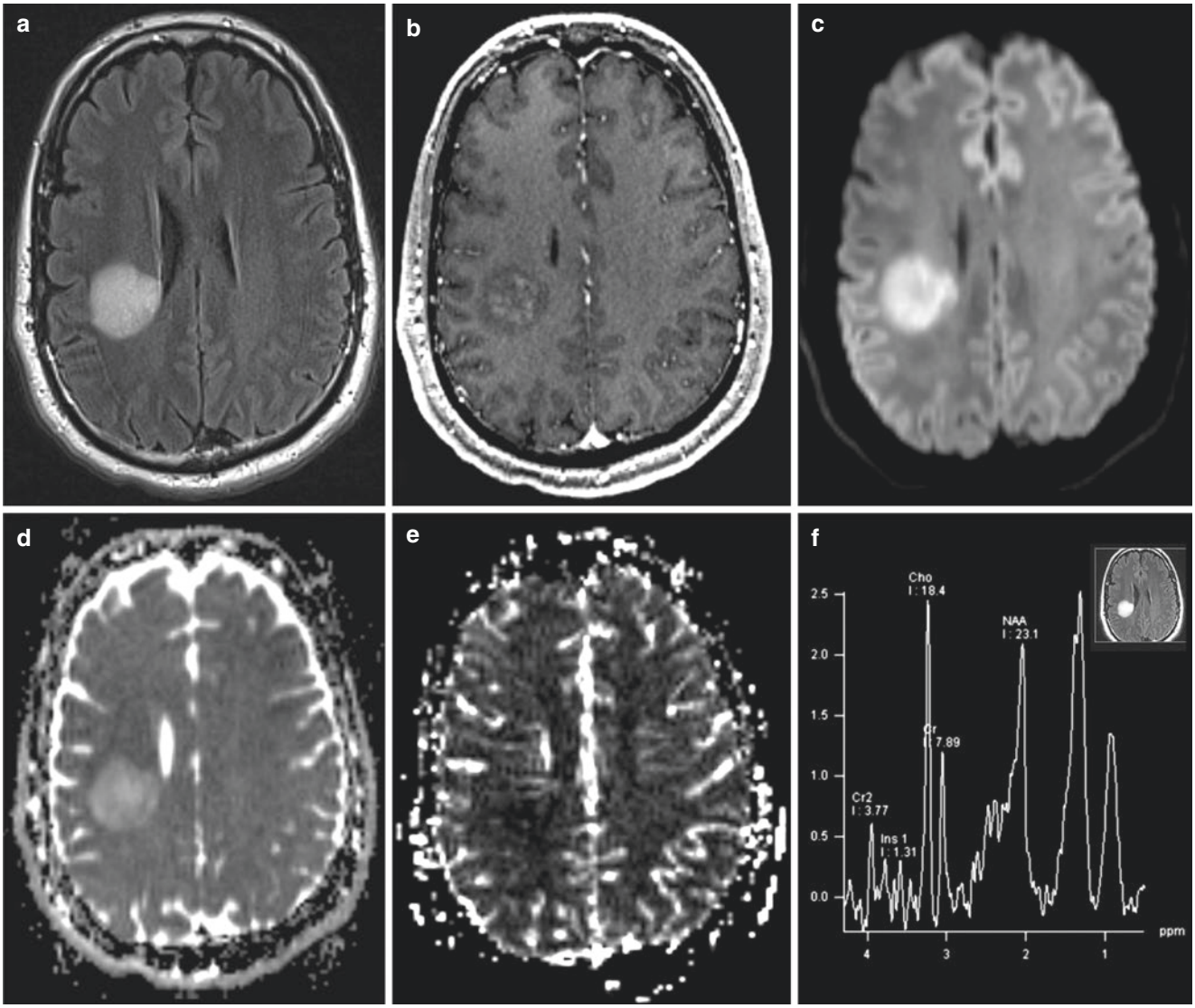

Fig. 12.6 Conventional and advanced MRI of a tumefactive demyelinating lesion in a patient subsequently diagnosed with multiple sclerosis. (**a**) Axial FLAIR image demonstrates a round area of hyperintensity in the right cerebral hemisphere. (**b**) Postcontrast T1-weighted image shows mild patchy areas of enhancement within the lesion. (**c**) DWI image shows high signal, which on the ADC map (**d**) is also hyperintense, suggesting facilitated diffusion (please note that tumefactive demyelinating lesions may sometimes have reduced diffusion as well). (**e**) CBV map derived from dynamic susceptibility contrast perfusion imaging demonstrates no increase in blood volume within the lesion. (**f**) MRI spectrum from a voxel placed within the lesion demonstrates elevated Cho/Cr and slightly elevated Cho/NAA ratios

[182, 183]. A recent study using DSC perfusion and DTI in 14 patients with brain infections and 21 patients with necrotic glioblastoma demonstrated that combined analysis of FA from the central core and maximum rCBV from the enhancing region provided the best classification model in distinguishing brain infections from necrotic GBMs, with a sensitivity of 91% and a specificity of 93% [183].

Pitfalls and Special Circumstances

Despite the utility of advanced MRI techniques to add to the diagnostic value of conventional MRI, it is important to recognize the limitations of these techniques and the pitfalls associated with acquisition, analysis, and interpretation of these techniques. Familiarity with the basic principles, tech-

nical limitations, and artifacts in each of these modalities is essential for successful integration with conventional MRI findings. Within each individual institution, both technical and personnel quality control is essential to ensure optimal use of these techniques. In the acquisition phase, development and implementation of sound imaging protocols is essential. MRI technologists will need additional training for implementing these protocols to minimize artifacts and inaccurate measurements. For example, optimal placement of spectroscopy voxels and grids in order to minimize the deleterious effects of proximity to or inclusion of air, fat, and bone is essential for optimal brain tumor spectroscopic imaging. Voxel size should be optimized to minimize partial volume effects around the tumor, but at the same time be large enough to ensure an adequate signal-to-noise ratio within the acquisition timeframe. Other techniques such as parallel imaging or nonechoplanar techniques may be employed to minimize the deleterious effect of susceptibility and geometric distortion in diffusion imaging. Adequate venous access and contrast injection rates affect the success and reliability of DSC perfusion MRI. Choice of pulse sequence, use of a preload dose of contrast, slice thickness, and use of parallel imaging are important considerations in DSC perfusion MRI.

Careful postprocessing analysis of spectroscopy and particularly perfusion data is also essential. The interpreting physician should have at least a basic understanding of the postprocessing steps involved. There are various models and processing methods available, and various commercial and noncommercial software packages have different interfaces and computational models for data analysis. Familiarity with the particular processing software and implementation of an internal institutional quality control of the postprocessing steps is important. Better curve fitting and baseline correction can improve the quality of spectroscopy data. Most institutions do not routinely perform quantitative spectroscopy, which requires a high level of understanding of the nuances behind MR spectroscopy, has its own challenges, and can be very time-consuming. There are various methods for perfusion imaging data analysis, application of corrections, and perfusion map reconstruction. Anecdotally, a simple but common mistake that the authors have observed in the processing of perfusion data is incorrect selection and placement of the various time points on the time concentration curves for perfusion map calculation. Visual inspection of the source time-signal intensity curves is important to assess excessive susceptibility artifacts, motion artifacts, bolus rate and timing, and correct processing of DSC perfusion MRI data, since many artifacts cannot be adequately assessed by looking at the postprocessed perfusion parameter maps.

Caution must be exercised in interpretation of diffusion and perfusion imaging when there are hemorrhagic areas within tumors. Large areas of hemorrhage may negatively affect accurate rCBV measurement. Caution must be exercised in interpreting diffusion-weighted imaging in the presence of hemorrhage. This could potentially affect differentiation of hemorrhagic brain tumors and abscesses. Significant areas of hemorrhage and calcification may also degrade MR spectroscopy and preclude obtaining a diagnostic spectrum. Detection of small highly perfused tumors in very superficial areas or within the gray matter can be difficult since the CBV of gray matter is already relatively high in normal brain. Differentiating subacute infarcts from brain tumors can occasionally be problematic, since there may be significant edema and mass effect in and around the area of infarct, and there may be heterogeneous reduced diffusion within the area of infarct itself. The patient's clinical history and course is often helpful in this distinction. Immunosuppressed patients with CNS lymphoma may have more peripherally enhancing lesions rather than solid enhancement, and may mimic high-grade primary neoplasm and other lesions. The clinical history of immunosuppression or HIV disease would be quite helpful in these patients. The use of high dose steroids can affect the enhancement and potentially perfusion characteristics of tumors, and therefore knowledge of the patient's "steroid status" is helpful for more accurate interpretation of brain tumor MRI exams.

One common diagnostic pitfall in the imaging of brain tumors is differentiating high-grade and low-grade oligodendrogliomas. Low-grade oligodendrogliomas may enhance and high-grade oligodendrogliomas may not show contrast enhancement [184]. MR perfusion imaging in oligodendrogliomas also can be confusing, as low-grade oligodendrogliomas may have elevated blood volume, mimicking high-grade tumor [134, 185]. An example of low-grade oligodendroglioma with high blood volume within the tumor is shown in Fig. 12.7.

Another potential pitfall is the presence of the large veins or developmental venous anomalies (venous angiomas) in the vicinity of brain masses. The presence of developmental venous anomalies can alter perfusion MRI parameters in the area and sometimes pose as areas of increased rCBV, potentially mimicking hypervascular tumor [186]. Similar increases in rCBV may occasionally be observed within capillary telangiectasias.

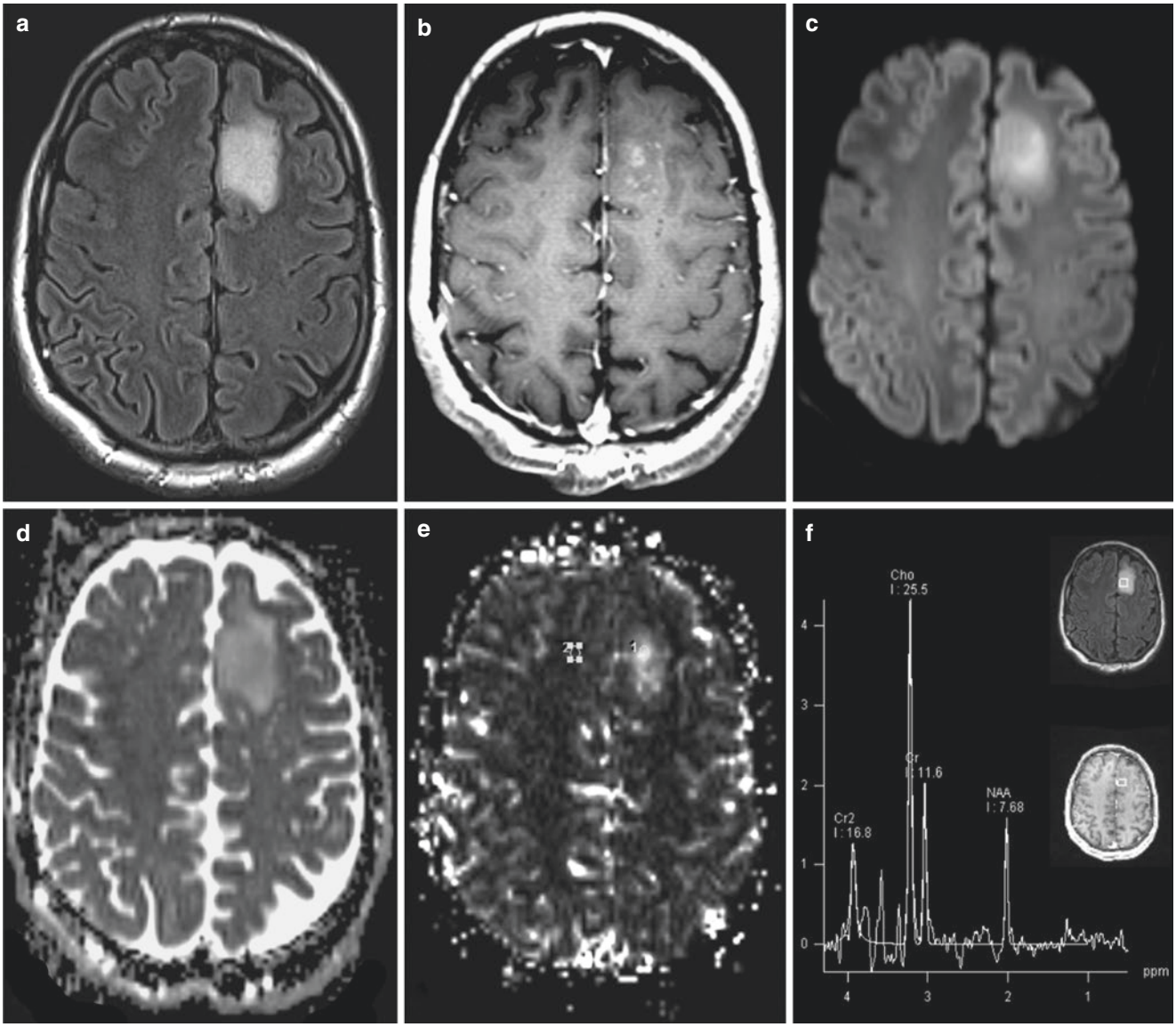

Fig. 12.7 Conventional and advanced MRI in a patient with grade II oligodendroglioma with 1p/19q chromosomal codeletion. (**a**) Axial FLAIR image demonstrates a hyperintense mass lesion in the left frontal lobe. (**b**) Postcontrast T1-weighted images demonstrate small faint areas of enhancement within the mass. DWI images (**c**) and ADC maps (**d**) do not show reduced diffusion in the mass. (**e**) CBV map from dynamic susceptibility contrast imaging demonstrates elevated blood volume within the mass compared to the contralateral white matter (see regions of interest measurements). In this particular case, the ratio was approximately 3.5. Low-grade oligodendrogliomas may enhance and have elevated blood volume within the tumor. (**f**) MRS performed with TE = 135 shows elevated Cho/Cr and Cho/NAA ratios

Pediatric Brain Tumors

There are important differences between pediatric and adult brain tumors. As such, the previously described diagnostic algorithm for characterization of intra-axial brain tumors in adults may not apply to many pediatric brain tumors. For example, pilocytic astrocytomas are one of the most common pediatric brain tumors, and despite being grade I tumors, a large percentage of these tumors partially enhance with gadolinium contrast and few could also demonstrate some increased blood volume on perfusion imaging, mimicking the enhancement and perfusion characteristics of adult high grade gliomas [187]. The most common pediatric posterior fossa tumors are pilocytic astrocytomas, medulloblastomas, and ependymomas. There can be considerable conventional imaging overlap, especially between ependymomas and medulloblastoma. In a study of pediatric cerebellar tumors, it was shown that comparison of NAA/Cho and Cr/Cho ratios by MR spectroscopy can reasonably differentiate between these three tumors [188]. Medulloblastoma typically has very high choline compared to creatine and NAA. In another study, elevated Taurine on MRS (at 3.4 ppm) was shown to

be significantly elevated and useful in the differentiation of medulloblastoma from other pediatric brain tumors, although reliable detection of Taurine is not trivial [189].

Diffusion-weighted imaging can be helpful in the differentiation of medulloblastoma from ependymomas or pilocytic astrocytomas in the cerebellum (Fig. 12.8). Both medulloblastoma and the less common atypical teratoid rhabdoid tumors (ATRT) often demonstrate restricted diffusion in their solid components. However, anaplastic ependymomas can also sometimes demonstrate restricted diffusion. Rumboldt et al. showed that quantitative ADC measurements, and also tumor ADC ratios with respect to normal white matter can differentiate posterior fossa pilocytic astrocytomas, ependymomas, and medulloblastomas/ATRT [190]. Another small study concluded that quantitative ADC ratios correlated reasonably well with pediatric tumor classifications into low grade gliomas, embryonal tumors, and non-embryonal high grade tumors [191]. In another small study of supratentorial pediatric brain tumors, it was shown that patients with lower NAA/Cho and Cr/Cho ratios have poorer prognosis [192]. This prognostic significance of the Cho/NAA ratio was confirmed in another cohort of pediatric brain tumors [193]. In a study of ASL perfusion in pediatric tumors, there was 77–88% grading accuracy in combing per-

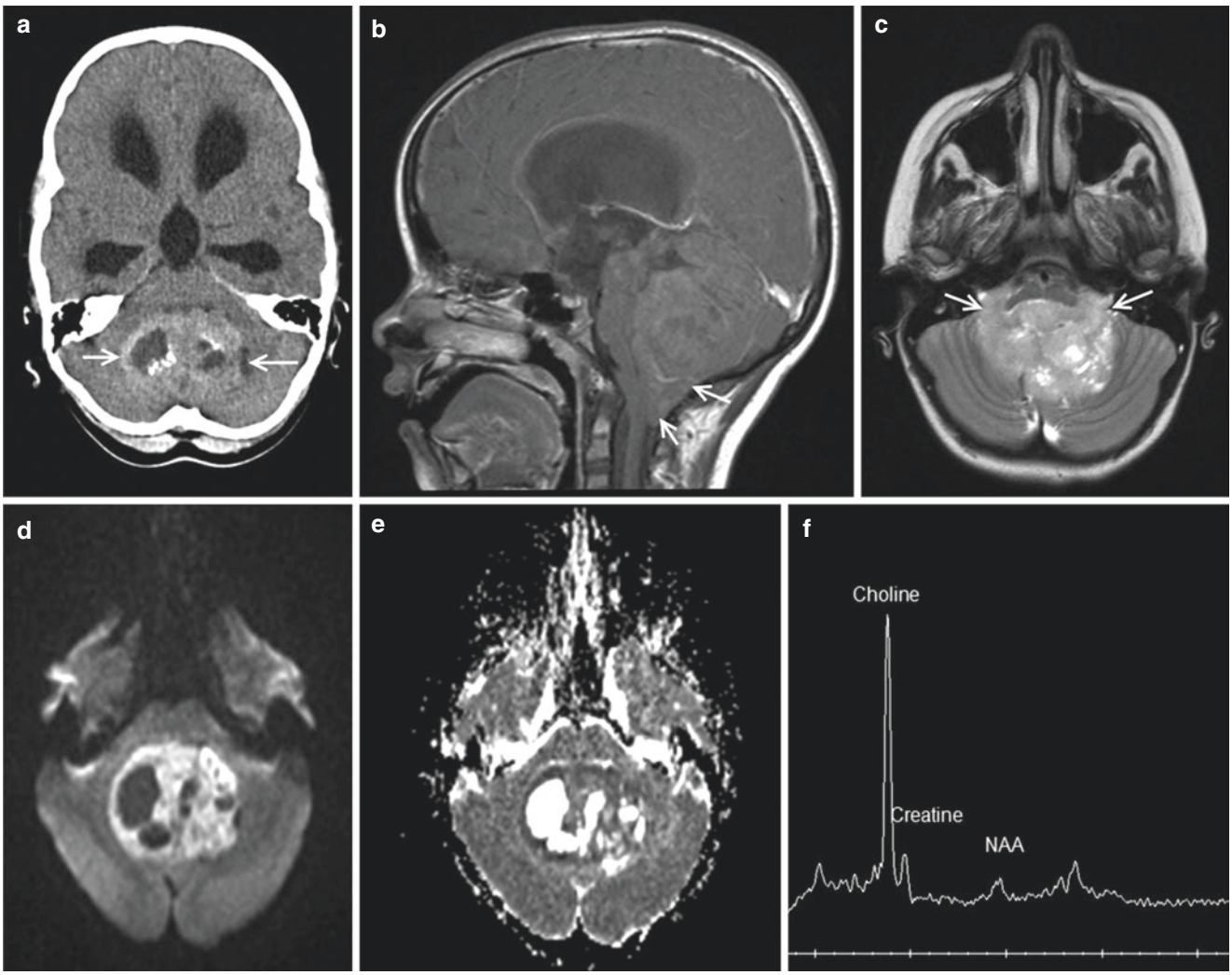

Fig. 12.8 Conventional and advanced MRI in a pediatric patient with a medulloblastoma. (**a**) Axial CT scan demonstrates a relatively hyperdense mass in the posterior fossa (arrows), along with cystic components and calcifications. Hyperdensity in the solid portion of pediatric posterior fossa masses is suggestive of a high nuclear/cytoplasm ratio. (**b**) Sagittal T1-weighted MRI demonstrates a large mass, but it is difficult to determine whether it is arising from within the ventricle or vermis. Portions of the mass are protruding way down through foramen Magendie into the cervical canal (arrows) with mass effect on the brainstem. (**c**) Axial T2-weighted image shows a T2 hyperintense mass with portions of the mass protruding out from the bilateral foramina of Luschka (arrows). Classically this "toothpaste-like" appearance has been described with ependymomas, but can be seen in large medulloblastomas as well. (**d**) DWI images show high signal within the solid portions of the mass, confirmed to indeed be due to restricted diffusion on the ADC maps (**e**). (**f**) MRS spectroscopy demonstrates very marked elevation of the Cho/Cr and Cho/NAA ratio, also a feature often seen in medulloblastoma

fusion and degree of contrast enhancement in assessing pediatric low and high grade neoplasms [194].

Post-treatment Imaging

In the case of high-grade gliomas, a common clinical scenario is differentiation of post-treatment effects from tumor recurrence, which can be difficult as they may clinically present similarly and also have a similar appearance on conventional MRI. Contrast enhancement, edema, and mass effect can be seen with post-treatment effects mimicking recurrent tumor contrast enhancement [159, 195]. Another complicating factor is that in many cases, recurrent neoplasm and post-treatment effects can co-exist in the same or nearby regions, with varying proportions [196]. Integrating various advanced imaging techniques with conventional MRI has potential to more accurately determine whether an enhancing region is due to predominately high-grade tumor recurrence or post-treatment effects. This differentiation has become more important since the addition of concurrent and consolidative regimes of temozolomide (TMZ) to radiation treatment as the standard of care for GBM, [197] which has also resulted by an increasing incidence of pseudoprogression (PsP). PsP is an early post-treatment effect which is most commonly seen in the first 3 months to up to 6 months after chemoradiation and demonstrates as increasing enhancement in the surgical bed which subsides in subsequent studies without any change in treatment. This is in contrast to classic radiation necrosis which is typically a late effect usually occurring 9–12 months or even years following photon-based radiation therapy, and which usually stabilizes or worsens rather than showing spontaneous resolution in contrary to PsP [198–200]. It has been shown that approximately 50% of the high grade glioma patients treated with standard chemoradiation can develop increasing enhancement in the surgical bed concerning for progression: however, in approximately 40% of patients, the enhancement improves or stabilize on subsequent studies indicating an approximately 20% incidence of PsP in high-grade gliomas patients treated with chemoradiation [201]. The distinction of PsP from true progression becomes more important noting that multiple studies demonstrated improved survival in patients who have PsP [202, 203] even when accounting for MGMT status [204], indicating that PsP can be a potential marker of enhanced antitumor efficacy. As such, it would be important to differentiate these two entities by imaging as PsP indicates success of the current treatment while true tumor progression warrant a change or treatment and even another resection.

An early study showed that rCBV >2.6 (relative to contralateral side) is consistent with recurrent tumor and rCBV<0.6 is consistent with radiation necrosis. rCBV values between 0.6 and 2.6 were indeterminate [205]. Hu and colleagues used image-guided neuro- navigation during surgical resection to correlate directly specimen histopathology and DSC rCBV measurements in high-grade glioma patients previously treated with multimodality therapy, and presenting with new enhancing lesions. They reported that in the post-treatment radiation effect group, rCBV values ranged from 0.20 to 0.71, and recurrent tumor rCBV measurements ranged from 0.55 to 4.64. Using a threshold value of 0.71, they were able to differentiate the histopathologic groups with a sensitivity of 91.7% and specificity of 100% [206]. In a more recent study, a cut off value of $rCBV_{max}$ = 2.77 only provided 82% sensitivity and 63% specificity to differentiate PsP from true progression and mixed tissue [207]. Overall, it has repeatedly been shown that perfusion is lower in post-treatment effects compared to tumor progression; however, the optimal threshold has yet to be determined and validated on prospective studies. A recent study evaluating 19 patients GBM with progressive enhancement on post chemoradiation MRI demonstrated that mean rCBV at the initial MRI did not differ significantly between PsP and true progression; however, change in rCBV at first subsequent follow-up and the overall linear trend in rCBV after initial progressive enhancement was significantly between PsP and true progression [208]. Finally, in a study of 31 patients (15 recurrent tumor and 16 radiation necrosis) with glioblastoma, Hu et al. trained a one-class-support vector machine classifier using a radiation necrosis training set and subsequently tested the classifier. They found a high sensitivity (89.91%) and speci-

ficity (93.72%) of optimized classifier for pseudoprogression and the area under the ROC curve was 0.9439 [209].

DCE MRI using both pharmacokinetic modeling and analysis of the area under the signal intensity curve has also been used to differentiate true progression from pseudoprogression in multiple studies. In a retrospective study of 37 patients with glioblastoma post-chemoradiation, pseudoprogression patients demonstrated lower Vp and Ktrans values, with a mean Vp cutoff <3.7 having 85% sensitivity and 79% specificity for pseudoprogression [210]. In a prospective study of 33 patients with glioblastoma who were followed post-chemoradiation, Yun et al. demonstrated that mean Ktrans and Ve were higher in true progression compared to pseudoprogression patients, and that mean Ktrans was the only independently differentiating variable [211]. Surprisingly the Vp was not significantly different between the true progression and pseudoprogression groups which could be secondary to short acquisition time in this study resulting in underestimation of Vp [212]. Bisdas et al. prospectively compared pharmacokinetic modeling and the initial area under the signal intensity curve (iAUC) and demonstrated that both Ktrans and iAUC were significantly higher in the recurrent glioma group than in the radiation necrosis group [213]. Finally Chung et al. used a bimodal histogram analysis of AUCR derived from DCE MRI and demonstrated that ratio of the initial area under the time signal intensity curve to the final AUC to be the best single predictor of recurrent GBM [214].

ASL imaging has also been applied to address the post-treatment changes in gliomas. In a study of 22 patients with recurrent high-grade glioma, ASL demonstrated hyperperfusion in all recurrent cases with mean CBF ratio 3.37 (±1.71) and there was a positive correlation between CBF and percentage of tumor [215]. In a study of 21 patients with post-treatment glioma using both ASL and DSC imaging, the normalized ASL-CBF ratio was higher in patient with recurrence (4.45 ± 2.72) compared to postradiation changes (1.22 ± 0.61) ($p < 0.01$). Also, the normalized rCBV ratio was also significantly higher in patients with recurrence (3.38 ± 2.08) compared to postradiation changes (1.09 ± 0.55). They also found a close linear correlation was found between the ASL and DSC MRI in differentiation of recurrent glioma from radiation injury [216]. In a retrospective study of 117 patients with GBM post-chemoradiation, Choi et al. used a semi-quantitative grading system based on comparing tumor perfusion signal intensity to the white matter (grade I), gray matter (grade II), and blood vessels (grade III) on ASL imaging and correlated the ASL grade with histogram parameters derived from DSC perfusion MRI. They found that adjunctive ASL produced eight (12.9%) more accurate results than DSC perfusion MRI alone and concluded that ASL improves the diagnostic accuracy of DSC perfusion MRI in differentiating pseudoprogression from early tumor progression [217]. Finally in a recent study, Razel et al. demonstrated that combined ASL and DTI metrics of the enhancing lesion revealed AUC of 0.98, accuracy of 95% to differentiate recurrent/residual gliomas from post-radiation changes [218].

On diffusion imaging, ADC values of radiation necrosis generally tend to be higher than in recurrent tumor tissue, though there is overlap and this is not a very specific finding [97, 219]. Multiple studies have assessed value of MR spectroscopy in distinguishing between radiation necrosis and recurrent gliomas [22, 97]. In one study, a Cho/Cr ratio greater than 1.3 was highly suggestive of tumor recurrence [220]. The combination of MR spectroscopy and DWI has been used in multiple studies to differentiate recurrent rumor from post-treatment effects [221, 222]. In a study of 55 patients with glioma, Zeng et al. demonstrated that based on discriminant analysis of Cho/NAA, Cho/Cr, and ADC ratio, 96.4% of total subjects were correctly classified compared to only 85.5% of subjects using the MR spectroscopy data [222]. In a recent study using DWI and DSC perfusion imaging in 35 patients with GBM, combined histogram analysis of ADC values and relative cerebral blood volume was the best predictor of true tumor progression and survival with a sensitivity of 82% and a specificity of 100% [223]. Wang et al. showed that the best model to distinguish true progression from non–true progression (pseudoprogression and mixed) consisted of fractional anisotropy, linear anisotropy coefficient, and maximum rCBV, resulting in an area under the curve of 0.905 [207]. An example of a patient with predominant radiation necrosis months after treatment is shown in Fig. 12.9 and a patient with pseudoprogression is shown in Fig. 12.10.

Recent use of antiangiogenesis agents and vascular endothelial growth factor (VEGF) receptor signaling pathway

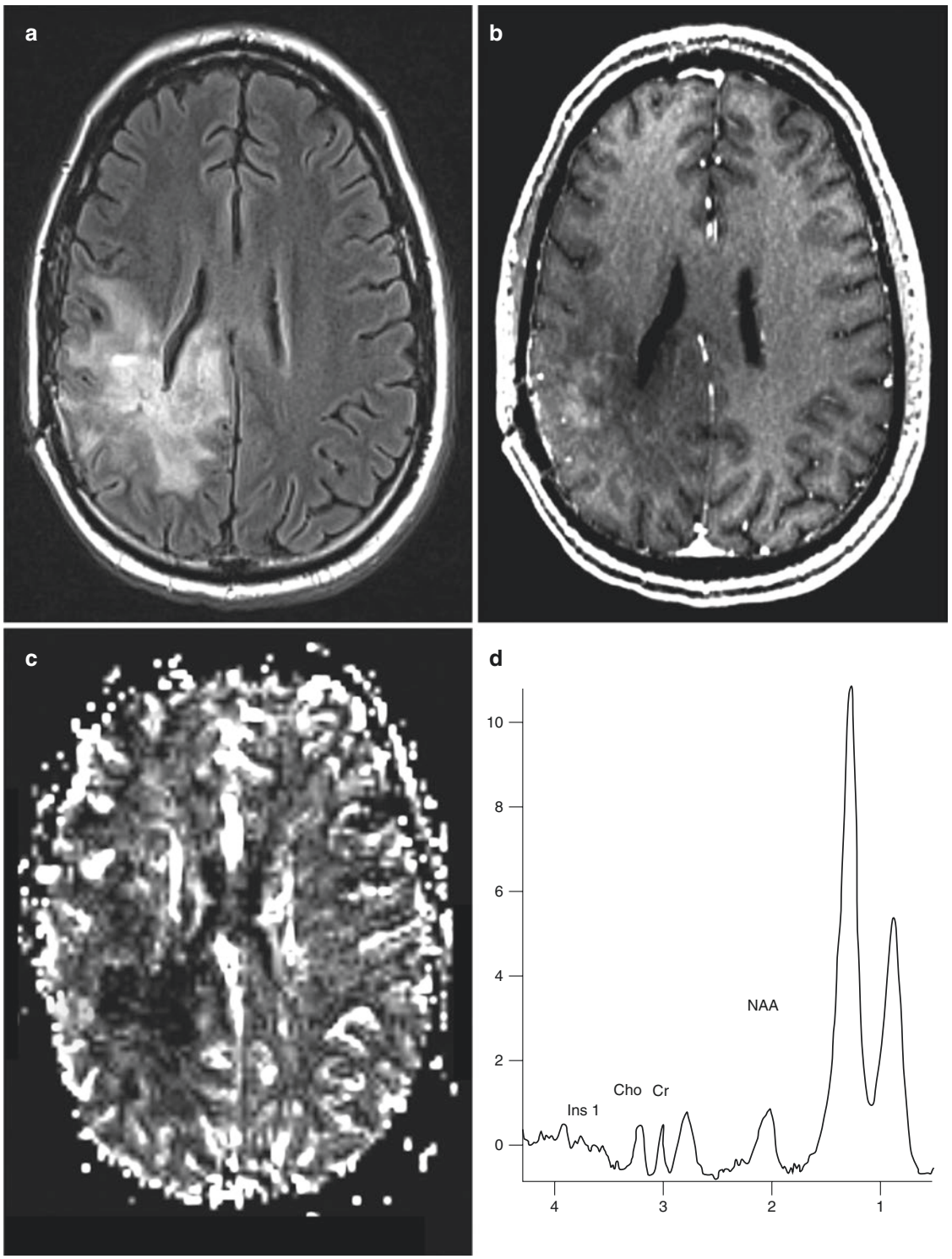

Fig. 12.9 Imaging findings in a patient with a history of glioblastoma status post surgery and radiation therapy months earlier, who now presents with progressive left-sided symptoms and new enhancement in the right cerebral hemisphere. (**a**) Axial FLAIR image demonstrates signal abnormality in the right posterior frontal and parietal lobes (which had slightly increased compared to an MRI 3 months earlier). (**b**) Postcontrast T1-weighted image demonstrates faint enhancement in a portion of the area of signal abnormality (which was new). At this point the differential diagnosis was radiation necrosis versus recurrent tumor. (**c**) CBV map from dynamic susceptibility contrast imaging demonstrates low blood volume in the area of enhancement. (**d**) MRS spectrum demonstrates elevated lipid-lactate, relatively low concentration of other metabolites and no increase in Cho/Cr or Cho/NAA ratios. The advanced imaging findings suggest that the predominant process in this patient is treatment change and radiation necrosis

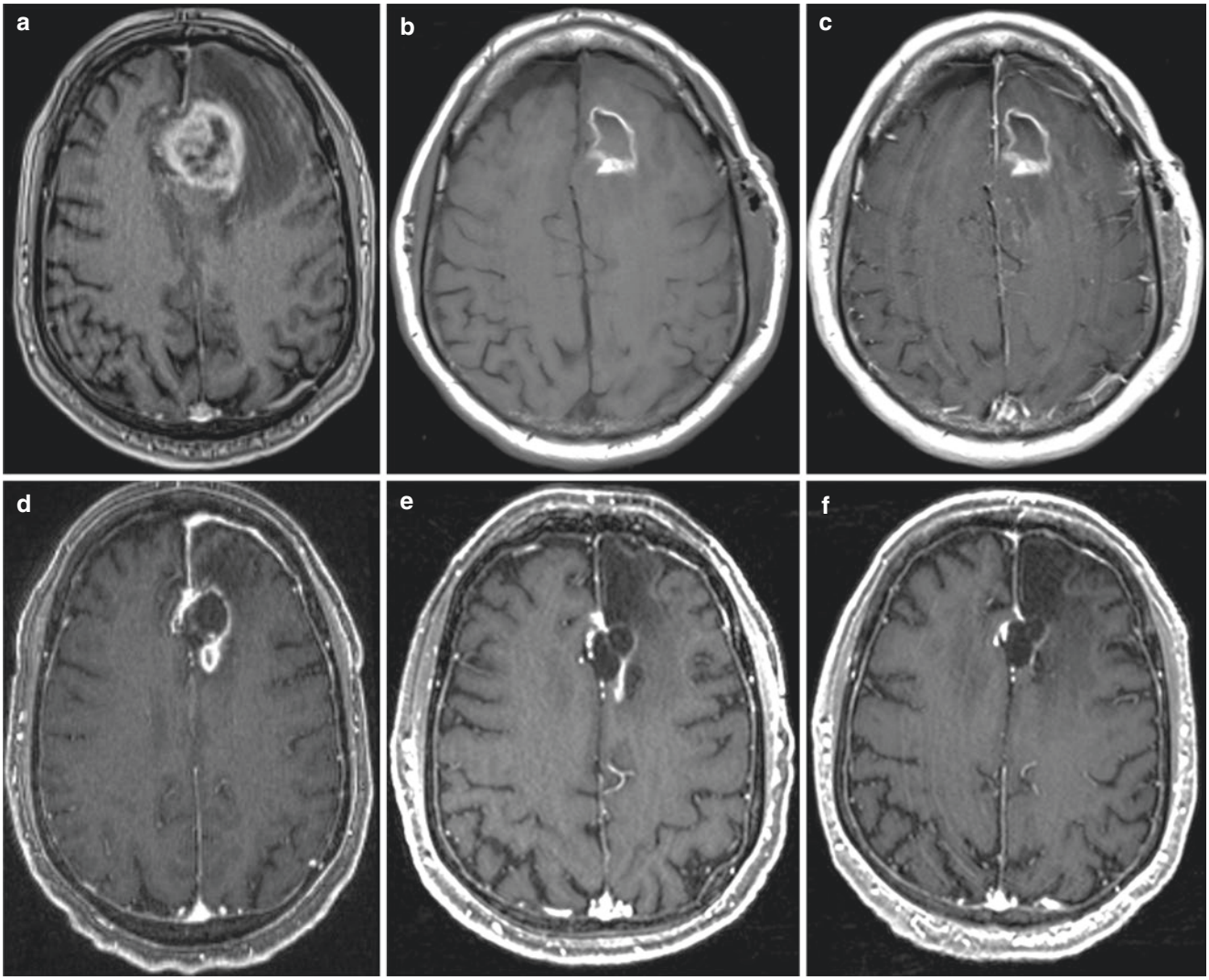

Fig. 12.10 Pseudoprogression in a patient with glioblastoma. (**a**) The preoperative T1-weighted postcontrast MRI shows a large left frontal enhancing mass. Immediate postoperative precontrast (**b**) and postcontrast (**c**) images show no definite residual enhancing mass beyond postoperative blood products. (**d**) Three months into the start of radiation and Temozolomide therapy, there has been development of a nodular area of enhancement along the posterior aspect of the resection cavity. Without any new treatment, this area of enhancement gradually resolved at 6 months (**e**) and 9 months (**f**), confirming pseudoprogression

inhibitors for brain neoplasms can complicate the follow-up imaging interpretation of these tumors [224, 225]. Use of these agents can change the vascularity of tumors and cause relative normalization of the vessels, resulting in decreased leakage of contrast. The response may at times be specific to the vessels only, rather than an actual tumor size, and therefore this phenomenon is also referred to as "pseudoresponse." In a subset of patients treated with antiangiogenic agents there may be nonenhancing tumor progression without evidence of an increase in tumor vascularity or even decreased enhancement [113, 226]. Attention to other conventional imaging sequences especially fluid attenuation inversion recovery (FLAIR) can demonstrate tumor progression in these patients in spite of decreased enhancement (Fig. 12.11).

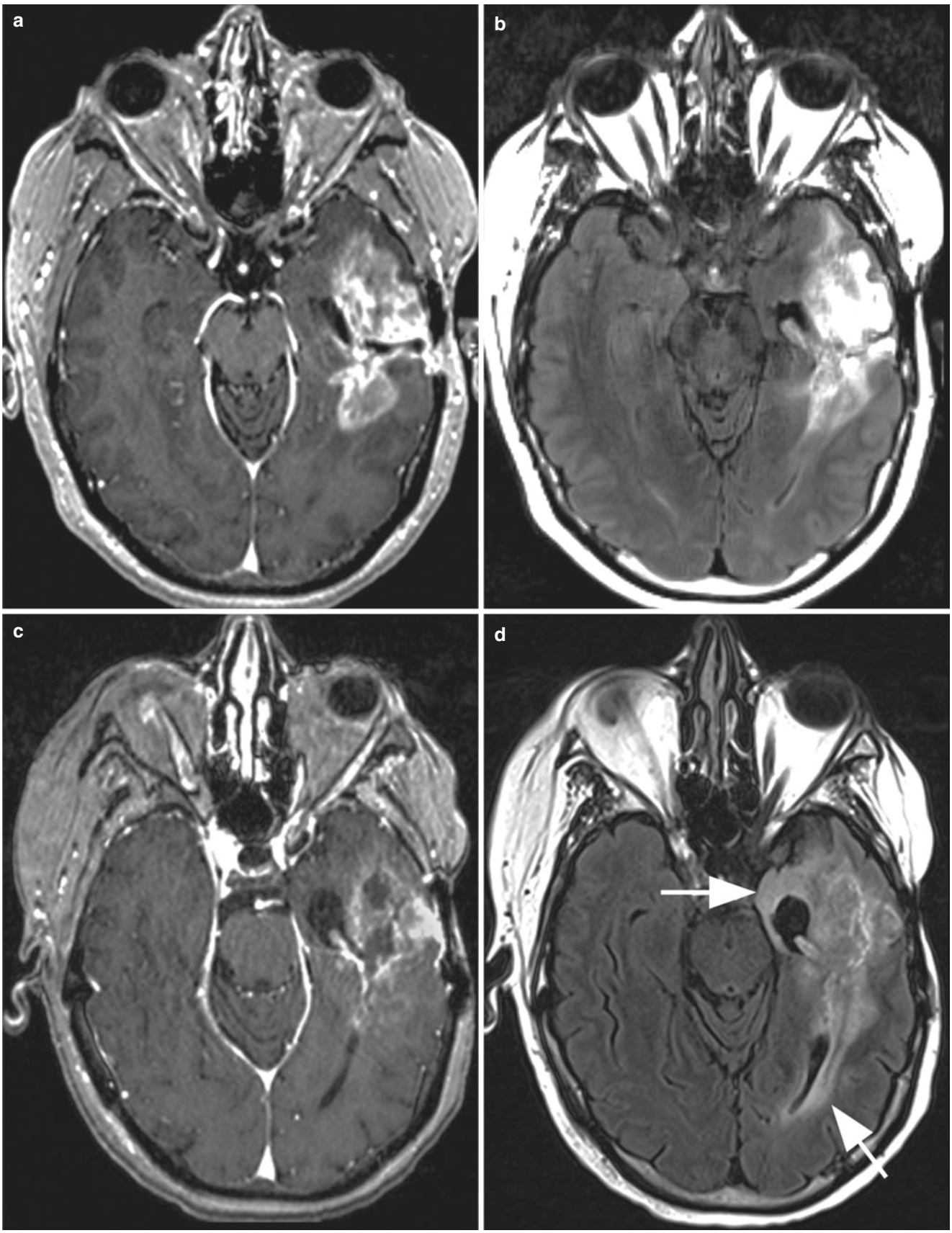

Fig. 12.11 Pseudoresponse in a postoperative patient with glioblastoma receiving antiangiogenic treatment. There is an enhancing mass in the left temporal lobe on postcontrast T1-weighted (**a**) and FLAIR (**b**) images. Follow-up months after antiangiogenic treatment show decrease in enhancing tumor (**c**), but there has been increase in infiltrative tumor on FLAIR images (**d**, arrows)

Current Challenges and Future Directions

Traditional research on imaging findings of brain tumors has been based on the concept of radiologic-pathologic correlation, trying to develop imaging criteria and then adjusting them in order to match the anatomical pathology of grossly resected tumor tissue. Recent advances in imaging have resulted in a multitude of functional imaging methods for assessment of brain tumors. Although these types of studies have been somewhat successful and have many times led to better diagnostic guidelines, the conclusions have always had considerable exceptions and often disappointing accuracies. Nevertheless, imaging studies have other advantages as well. While in-vitro data are very useful to describe particular features of brain tumors, advanced MRI techniques can provide data about several independent aspects of brain tumor biology. Advanced MRI techniques can produce an impressive array of in vivo data reflecting tumor cellularity, metabolism, invasiveness, vascular density, permeability, and vessel reactivity to different challenges [227], many of which cannot be effectively addressed by in-vitro studies of excised or biopsied tissue. Advanced imaging techniques can give us insights into several aspects of brain tumors that cannot be adequately addressed by conventional histopathologic criteria. Good examples of this potential role of advanced imaging is the prediction of survival in high-grade brain tumors and also prediction of time to progression in low-grade gliomas, both of which has been demonstrated using perfusion imaging [146, 228]. In addition, a number of recent reports have directly correlated advanced imaging findings with biologic features such as molecular genotype and phenotype [229], and even used advanced imaging features to monitor novel treatments [230].

In the past, the methodology used in brain tumor studies was determination of accuracy of each of the advanced imaging methods. Multimodality imaging as a combination of advanced imaging techniques can be a potential problem solver that provides us with new information that is not achievable by any one of them in isolation. A classic example of successful use of multimodality imaging is in oligodendroglioma grading. Cerebral blood volume (rCBV) measurements from dynamic susceptibility-weighted contrast-enhanced MR imaging have been shown to correlate with glioma grade; however, the confounding effect of low-grade oligodendroglioma with high perfusion will significantly decrease the specificity of perfusion imaging in glioma grading [134]. Chawla et al. tried to solve this problem by combining perfusion and spectroscopy data. They used cerebral blood flow (CBF) maps generated by arterial spin labeling (ASL) to guide voxel-by voxel analysis of MRS to evaluate the efficacy of this method in grading of oligodendroglioma [135]. They demonstrated a significant difference in normalized choline ratio between high- and low-grade oligodendroglioma limited to only the highly perfused regions of the tumors (defined as areas with CBF more than one standard deviation higher than the contralateral white matter). This study is just an example that shows the value of thoughtfully designed multimodality imaging studies.

Use of newer multimodality registration techniques and multivariable pattern classification techniques has allowed even greater quantitative in vivo characterization of brain tumor tissues [231, 232]. Given the increasing trend in using machine learning and artificial intelligence in neuroradiology, investigators in multiple institutions are looking into the best combinations of imaging features to characterize post-treatment changes and more publications in near future are expected. Various published publications now purport to better classify brain tumors, delineate margins of infiltrating gliomas, differentiate true from pseudo-progression, and predict survival or recurrence better than conventional methods [233, 234]. By providing in vivo markers of spatial and molecular heterogeneity, machine learning tools have the potential to better stratify patients into tailored therapeutic pathways, in the hope of achieving personalized medicine. Although substantial challenges remain, radiologic practice is set to change considerably as AI technology is further developed and validated for clinical use. Application of various texture analysis (radiomics), imaging-genomic correlations (radiogenomics), and machine learning prognostic models have increased, but need more judicious application in order to prevent overfit models and poor generalizability across centers and protocols. One major factor contributing to poor generalizability of many advanced imaging studies of brain tumors is the lack of standardization of imaging protocols, analysis methods, and finally the implementation of these methods in clinical practice. This lack of standardization has, for example, led to inconsistent results when investigators tried to use different perfusion imaging protocols to answer similar questions [114]. There have been many recent attempts to standardize advanced imaging acquisition and analysis for brain tumor imaging trials [235–237].

Integration of conventional and advanced imaging data into existing histopathologic and molecular criteria may lead to better diagnostic and therapeutic guidelines and has the potential to improve patient care. Ideally, in the future we would be able to design models and software to analyze a variety of different imaging, pathologic, molecular, and genetic parameters of a given tumor and get "personalized" information about the biology, treatment responsiveness, and prognosis of the tumor. Big data collection and analytical approaches along with the use of validated and generalizable machine learning techniques have great potential for realizing these goals (Table 12.1).

Table 12.1 Selected articles on the utility of advanced imaging in characterization of intra-axial brain masses

Author	Title	Summary
Aronen et al., 1994 [128]	Cerebral blood volume maps of gliomas: comparison with tumor grade and histologic findings	This study demonstrated the difference in maximum CBV in high-grade and low-grade gliomas. It also showed that maximum CBV is associated with the degree of mitotic activity and vascularity of glial brain tumors on histology
Brunberg et al., 1995 [161]	In vivo MR determination of water diffusion coefficients and diffusion anisotropy: correlation with structural alteration in gliomas of the cerebral hemispheres	The study showed how quantitative diffusion-weighted imaging with apparent diffusion coefficients and diffusion anisotropy can distinguish between normal white matter, edema, necrosis/cyst formation, and solid enhancing tumor in patients with cerebral glioma
Knopp et al., 1999 [131]	Glial neoplasms: dynamic contrast-enhanced T2*-weighted MR imaging	The study demonstrated the use of rCBV in preoperative grading of gliomas and use of maximum rCBV in targeting stereotactic biopsy of lesions.
Moller-Hartmann et al., 2002 [23]	Clinical application of proton magnetic resonance spectroscopy in the diagnosis of intracranial mass lesions	This study was the largest head-to-head comparison of conventional MR imaging alone versus MR imaging and MRS for assessment of brain tumors. In assessing 176 patients, the authors reported that combining MRS with conventional MRI increases the diagnostic accuracy from 55% to 71%
Law et al., 2002 [39]	High-Grade Gliomas and Solitary Metastases: Differentiation by Using Perfusion and Proton Spectroscopic MR Imaging	The study demonstrated that rCBV and choline-to-creatine ratios in the peritumoral region can be used to distinguish high-grade gliomas and solitary metastases based on perfusion MRI and MRS
Guo et al., 2002 [69]	Lymphomas and high-grade astrocytomas: comparison of water diffusibility and histologic characteristics	This study demonstrated that in lymphomas and high-grade astrocytomas, the apparent diffusion coefficient on diffusion-weighted imaging correlates with tumor cellularity on histopathology
Hollingworth et al., 2006 [238]	A Systematic Literature Review of Magnetic Resonance Spectroscopy for the Characterization of Brain Tumors	The study systematically evaluates MRS in distinguishing metastasis versus high-grade tumor, high-grade versus low-grade tumor, recurrent tumor versus radiation necrosis, tumors versus non-neoplastic lesions, and evaluation of tumor extent. It also presents guidelines to help focus future research
Al-Okaili et al., 2007 [4]	Intraaxial brain masses: MR imaging-based diagnostic strategy--initial experience	The authors evaluated a proposed diagnostic imaging strategy algorithm for differentiation of intra-axial brain masses in adults and showed an 85–90% accuracy for preoperative characterization of intra-axial brain masses
Law et al., 2008 [146]	Gliomas: predicting time to progression or survival with cerebral blood volume measurements at dynamic susceptibility-weighted contrast-enhanced perfusion MR imaging	In this study, the authors sought to determine whether rCBV measurements can be used to predict clinical outcome in patients with glioma. It showed that rCBV on DSC perfusion imaging can be used to predict mean time to progression in patients with gliomas, independent of pathologic findings and tumor grade
Choi et al., 2012 [13]	2-hydroxyglutarate detection by magnetic resonance spectroscopy in IDH-mutated patients with gliomas	This paper demonstrated that IDH mutations in gliomas can be determined by detecting 2HG using particular MR spectroscopy acquisition and analysis methods
Ellingson et al., 2015 [236]	Consensus recommendations for a standardized Brain Tumor Imaging Protocol in clinical trials	This white paper presents the recommendations of a joint meeting between the FDA, National Cancer Institute, various imaging experts, biotech/pharmaceutical companies, clinical trials cooperative groups, and patient advocate groups to discuss imaging endpoints and specifications for creation of a standardized Brain Tumor Imaging Protocol (BTIP), along with recommended ranges of sequence parameters

References

1. Law M, Yang S, Wang H, et al. Glioma grading: sensitivity, specificity, and predictive values of perfusion MR imaging and proton MR spectroscopic imaging compared with conventional MR imaging. AJNR Am J Neuroradiol. 2003;24(10):1989–98.
2. Giannini C, Scheithauer BW, Weaver AL, et al. Oligodendrogliomas: reproducibility and prognostic value of histologic diagnosis and grading. J Neuropathol Exp Neurol. 2001;60(3):248–62.
3. Al-Okaili RN, Krejza J, Wang S, Woo JH, Melhem ER. Advanced MR imaging techniques in the diagnosis of intraaxial brain tumors in adults. Radiographics. 2006;26(Suppl 1):S173–89.
4. Al-Okaili RN, Krejza J, Woo JH, et al. Intraaxial brain masses: MR imaging-based diagnostic strategy—initial experience. Radiology. 2007;243(2):539–50.
5. Ross B, Bluml S. Magnetic resonance spectroscopy of the human brain. Anat Rec. 2001;265(2):54–84.
6. Marshall I, Wardlaw J, Cannon J, Slattery J, Sellar RJ. Reproducibility of metabolite peak areas in 1H MRS of brain. Magn Reson Imaging. 1996;14(3):281–92.
7. Podo F. Tumour phospholipid metabolism. NMR Biomed. 1999;12(7):413–39.
8. Li X, Lu Y, Pirzkall A, McKnight T, Nelson SJ. Analysis of the spatial characteristics of metabolic abnormalities in newly diagnosed glioma patients. J Magn Reson Imaging. 2002;16(3):229–37.
9. Kreis R, Ernst T, Ross BD. Development of the human brain: in vivo quantification of metabolite and water content with proton magnetic resonance spectroscopy. Magn Reson Med. 1993;30(4):424–37.
10. Hattingen E, Raab P, Franz K, Zanella FE, Lanfermann H, Pilatus U. Myo-inositol: a marker of reactive astrogliosis in glial tumors? NMR Biomed. 2008;21(3):233–41.
11. Fulham MJ, Bizzi A, Dietz MJ, et al. Mapping of brain tumor metabolites with proton MR spectroscopic imaging: clinical relevance. Radiology. 1992;185(3):675–86.
12. Castillo M, Smith JK, Kwock L. Correlation of myo-inositol levels and grading of cerebral astrocytomas. AJNR Am J Neuroradiol. 2000;21(9):1645–9.
13. Choi C, Ganji SK, DeBerardinis RJ, et al. 2-Hydroxyglutarate detection by magnetic resonance spectroscopy in IDH-mutated patients with gliomas. Nat Med. 2012;18(4):624–9.
14. Andronesi OC, Kim GS, Gerstner E, et al. Detection of 2-hydroxyglutarate in IDH-mutated glioma patients by in vivo spectral-editing and 2D correlation magnetic resonance spectroscopy. Sci Transl Med. 2012;4(116):116ra114.
15. Suh CH, Kim HS, Jung SC, Choi CG, Kim SJ. 2-Hydroxyglutarate MR spectroscopy for prediction of isocitrate dehydrogenase mutant glioma: a systemic review and meta-analysis using individual patient data. Neuro-oncology. 2018;20(12):1573–83.
16. Mishra AM, Gupta RK, Jaggi RS, et al. Role of diffusion-weighted imaging and in vivo proton magnetic resonance spectroscopy in the differential diagnosis of ring-enhancing intracranial cystic mass lesions. J Comput Assist Tomogr. 2004;28(4):540–7.
17. Lai PH, Hsu SS, Ding SW, et al. Proton magnetic resonance spectroscopy and diffusion-weighted imaging in intracranial cystic mass lesions. Surg Neurol. 2007;68(Suppl 1):S25–36.
18. Shih MT, Singh AK, Wang AM, Patel S. Brain lesions with elevated lactic acid peaks on magnetic resonance spectroscopy. Curr Probl Diagn Radiol. 2004;33(2):85–95.
19. Preul MC, Caramanos Z, Collins DL, et al. Accurate, noninvasive diagnosis of human brain tumors by using proton magnetic resonance spectroscopy. Nat Med. 1996;2(3):323–5.
20. Gajewicz W, Papierz W, Szymczak W, Goraj B. The use of proton MRS in the differential diagnosis of brain tumors and tumor-like processes. Med Sci Monit. 2003;9(9):MT97–105.
21. Devos A, Lukas L, Suykens JA, et al. Classification of brain tumours using short echo time 1H MR spectra. J Magn Reson. 2004;170(1):164–75.
22. Vuori K, Kankaanranta L, Hakkinen AM, et al. Low-grade gliomas and focal cortical developmental malformations: differentiation with proton MR spectroscopy. Radiology. 2004;230(3):703–8.
23. Moller-Hartmann W, Herminghaus S, Krings T, et al. Clinical application of proton magnetic resonance spectroscopy in the diagnosis of intracranial mass lesions. Neuroradiology. 2002;44(5):371–81.
24. Ando K, Ishikura R, Nagami Y, et al. Usefulness of Cho/Cr ratio in proton MR spectroscopy for differentiating residual/recurrent glioma from non-neoplastic lesions. Nippon Igaku Hoshasen Gakkai Zasshi. 2004;64(3):121–6.
25. Catalaa I, Henry R, Dillon WP, et al. Perfusion, diffusion and spectroscopy values in newly diagnosed cerebral gliomas. NMR Biomed. 2006;19(4):463–75.
26. Hawkes RC, Holland GN, Moore WS, Worthington BS. Nuclear magnetic resonance (NMR) tomography of the brain: a preliminary clinical assessment with demonstration of pathology. J Comput Assist Tomogr. 1980;4(5):577–86.
27. McKnight TR, Noworolski SM, Vigneron DB, Nelson SJ. An automated technique for the quantitative assessment of 3D-MRSI data from patients with glioma. J Magn Reson Imaging. 2001;13(2):167–77.
28. Kiricuta IC Jr. More "free water" fraction in rapidly growing tissue, WHY? Indian J Cancer. 1978;15(2):19–22.
29. Halpern MB. [Magnesium in the cerebral calcifications of the Sturge-Weber syndrome: a study using a Castaing electron probe]. C R Acad Sci Hebd Seances Acad Sci D. 1976;282(1):113–4.
30. Zonari P, Baraldi P, Crisi G. Multimodal MRI in the characterization of glial neoplasms: the combined role of single-voxel MR spectroscopy, diffusion imaging and echo-planar perfusion imaging. Neuroradiology. 2007;49(10):795–803.
31. Hall WA, Martin A, Liu H, Truwit CL. Improving diagnostic yield in brain biopsy: coupling spectroscopic targeting with real-time needle placement. J Magn Reson Imaging. 2001;13(1):12–5.
32. Dowling C, Bollen AW, Noworolski SM, et al. Preoperative proton MR spectroscopic imaging of brain tumors: correlation with histopathologic analysis of resection specimens. AJNR Am J Neuroradiol. 2001;22(4):604–12.
33. Imae T, Fasman GD, Hinkle PM, Tashjian AH Jr. Intrinsic tryptophan fluorescence of membranes of GH3 pituitary cells: quenching by thyrotropin-releasing hormone. Biochem Biophys Res Commun. 1975;62(4):923–32.
34. Zaner KS, Damadian R. NMR in cancer: IX. The concept of cancer treatment by NMR: a preliminary report of high resolution NMR or phosphorus in normal and malignant tissues. Physiol Chem Phys. 1975;7(5):437–51.
35. Biswas DK, Tashjian AH Jr. Intracellular site of prolactin synthesis in rat pituitary cells in culture. Biochem Biophys Res Commun. 1974;60(1):241–8.
36. Lukas L, Devos A, Suykens JA, et al. Brain tumor classification based on long echo proton MRS signals. Artif Intell Med. 2004;31(1):73–89.
37. McLaren EH, Hendricks S, Pimstone BL. Thyrotrophin responses to intravenous thyrotrophin-releasing hormone in patients with hypothalamic and pituitary disease. Clin Endocrinol (Oxf). 1974;3(2):113–22.
38. Chiang IC, Kuo YT, Lu CY, et al. Distinction between high-grade gliomas and solitary metastases using peritumoral 3-T magnetic resonance spectroscopy, diffusion, and perfusion imagings. Neuroradiology. 2004;46(8):619–27.
39. Law M, Cha S, Knopp EA, Johnson G, Arnett J, Litt AW. High-grade gliomas and solitary metastases: differentiation by using

perfusion and proton spectroscopic MR imaging. Radiology. 2002;222(3):715–21.
40. Hendrick D, Schwarz W, Pitzel S, Tiedemann H. Messenger ribonucleoprotein-directed globin synthesis in an embryonic brain cell-free system. Biochim Biophys Acta. 1974;340(3):278–84.
41. Chawla S, Zhang Y, Wang S, et al. Proton magnetic resonance spectroscopy in differentiating glioblastomas from primary cerebral lymphomas and brain metastases. J Comput Assist Tomogr. 2010;34(6):836–41.
42. Beaven MA, Jacobsen S, Horakova Z. Modification of the enzymatic isotopic assay of histamine and its application to measurement of histamine in tissues, serum and urine. Clin Chim Acta. 1972;37:91–103.
43. McKnight TR, von dem Bussche MH, Vigneron DB, et al. Histopathological validation of a three-dimensional magnetic resonance spectroscopy index as a predictor of tumor presence. J Neurosurg. 2002;97(4):794–802.
44. Piccoli F, Amore G, Bonavita V. Aspartate aminotransferase in brain tissue cultures. J Neurochem. 1969;16(10):1487–9.
45. Sheid B, Bilik E. S-adenosylmethionine synthetase activity in some normal rat tissues and transplantable hepatomas. Cancer Res. 1968;28(12):2512–5.
46. Wakabayashi T, Fujii M, Kajita Y, Natsume A, Maezawa S, Yoshida J. Advanced new neurosurgical procedure using integrated system of intraoperative MRI and neuronavigation with multimodal neuroradiological images. Nagoya J Med Sci. 2009;71(3–4):101–7.
47. Emanuel NM. Kinetics and the free-radical mechanisms of tumor growth. Ann N Y Acad Sci. 1973;222:1010–30.
48. Zaworski RE, Oyasu R. Lead concentration in human brain tissue: an autopsy study. Arch Environ Health. 1973;27(6):383–6.
49. Swartz HM, Mailer C, Ambegaonkar S, Antholine WE, McNellis DR, Schneller SJ. Paramagnetic changes during development of a transplanted AKR-J leukemia in mice as measured by electron spin resonance. Cancer Res. 1973;33(11):2588–95.
50. Trams EG. A rapid fluorometric assay for 2',3'-cyclic adenosine monophosphate 3'-phosphoesterhydrolase. J Neurochem. 1973;21(4):995–7.
51. Szent-Gyorgyi A. Bioelectronics and cancer. J Bioenerg. 1973;4(6):533–62.
52. Takanashi R. A pathological study on the juvenile type of chronic myeloid leukemia. Acta Pathol Jpn. 1972;22(3):489–508.
53. Yeh IB, Xu M, Ng WH, Ye J, Yang D, Lim CC. Central neurocytoma: typical magnetic resonance spectroscopy findings and atypical ventricular dissemination. Magn Reson Imaging. 2008;26(1):59–64.
54. Winkelman J, Slater G, Grossman J. The concentration in tumor and other tissues of parenterally administered tritium- and 14-C-labeled tetraphenylporphinesulfonate. Cancer Res. 1967;27(11):2060–4.
55. Wald LL, Nelson SJ, Day MR, et al. Serial proton magnetic resonance spectroscopy imaging of glioblastoma multiforme after brachytherapy. J Neurosurg. 1997;87(4):525–34.
56. Graves EE, Nelson SJ, Vigneron DB, et al. Serial proton MR spectroscopic imaging of recurrent malignant gliomas after gamma knife radiosurgery. AJNR Am J Neuroradiol. 2001;22(4):613–24.
57. Balmaceda C, Critchell D, Mao X, et al. Multisection 1H magnetic resonance spectroscopic imaging assessment of glioma response to chemotherapy. J Neurooncol. 2006;76(2):185–91.
58. Sankar T, Caramanos Z, Assina R, et al. Prospective serial proton MR spectroscopic assessment of response to tamoxifen for recurrent malignant glioma. J Neurooncol. 2008;90(1):63–76.
59. Murphy PS, Viviers L, Abson C, et al. Monitoring temozolomide treatment of low-grade glioma with proton magnetic resonance spectroscopy. Br J Cancer. 2004;90(4):781–6.
60. Plotkin M, Eisenacher J, Bruhn H, et al. 123I-IMT SPECT and 1H MR-spectroscopy at 3.0 T in the differential diagnosis of recurrent or residual gliomas: a comparative study. J Neurooncol. 2004;70(1):49–58.
61. Traber F, Block W, Flacke S, et al. 1H-MR Spectroscopy of brain tumors in the course of radiation therapy: use of fast spectroscopic imaging and single-voxel spectroscopy for diagnosing recurrence. Rofo. 2002;174(1):33–42.
62. Lichy MP, Henze M, Plathow C, Bachert P, Kauczor HU, Schlemmer HP. Metabolic imaging to follow stereotactic radiation of gliomas—the role of 1H MR spectroscopy in comparison to FDG-PET and IMT-SPECT. Rofo. 2004;176(8):1114–21.
63. Zeng QS, Li CF, Zhang K, Liu H, Kang XS, Zhen JH. Multivoxel 3D proton MR spectroscopy in the distinction of recurrent glioma from radiation injury. J Neurooncol. 2007;84(1):63–9.
64. Reddy JS, Mishra AM, Behari S, et al. The role of diffusion-weighted imaging in the differential diagnosis of intracranial cystic mass lesions: a report of 147 lesions. Surg Neurol. 2006;66(3):246–50; discussion 250–241.
65. Park SH, Chang KH, Song IC, Kim YJ, Kim SH, Han MH. Diffusion-weighted MRI in cystic or necrotic intracranial lesions. Neuroradiology. 2000;42(10):716–21.
66. Biousse V, Newman NJ, Hunter SB, Hudgins PA. Diffusion weighted imaging in radiation necrosis. J Neurol Neurosurg Psychiatry. 2003;74(3):382–4.
67. Tung GA, Evangelista P, Rogg JM, Duncan JA III. Diffusion-weighted MR imaging of rim-enhancing brain masses: is markedly decreased water diffusion specific for brain abscess? AJR Am J Roentgenol. 2001;177(3):709–12.
68. Malhotra HS, Jain KK, Agarwal A, et al. Characterization of tumefactive demyelinating lesions using MR imaging and in-vivo proton MR spectroscopy. Mult Scler. 2009;15(2):193–203.
69. Guo AC, Cummings TJ, Dash RC, Provenzale JM. Lymphomas and high-grade astrocytomas: comparison of water diffusibility and histologic characteristics. Radiology. 2002;224(1):177–83.
70. Toh CH, Chen YL, Hsieh TC, Jung SM, Wong HF, Ng SH. Glioblastoma multiforme with diffusion-weighted magnetic resonance imaging characteristics mimicking primary brain lymphoma. Case report. J Neurosurg. 2006;105(1):132–5.
71. Calvar JA, Meli FJ, Romero C, et al. Characterization of brain tumors by MRS, DWI and Ki-67 labeling index. J Neurooncol. 2005;72(3):273–80.
72. Higano S, Yun X, Kumabe T, et al. Malignant astrocytic tumors: clinical importance of apparent diffusion coefficient in prediction of grade and prognosis. Radiology. 2006;241(3):839–46.
73. Lee EJ, Lee SK, Agid R, Bae JM, Keller A, Terbrugge K. Preoperative grading of presumptive low-grade astrocytomas on MR imaging: diagnostic value of minimum apparent diffusion coefficient. AJNR Am J Neuroradiol. 2008;29(10):1872–7.
74. Sugahara T, Korogi Y, Kochi M, et al. Usefulness of diffusion-weighted MRI with echo-planar technique in the evaluation of cellularity in gliomas. J Magn Reson Imaging. 1999;9(1):53–60.
75. Murakami R, Hirai T, Sugahara T, et al. Grading astrocytic tumors by using apparent diffusion coefficient parameters: superiority of a one- versus two-parameter pilot method. Radiology. 2009;251(3):838–45.
76. Tozer DJ, Jager HR, Danchaivijitr N, et al. Apparent diffusion coefficient histograms may predict low-grade glioma subtype. NMR Biomed. 2007;20(1):49–57.
77. Jenkinson MD, Smith TS, Brodbelt AR, Joyce KA, Warnke PC, Walker C. Apparent diffusion coefficients in oligodendroglial tumors characterized by genotype. J Magn Reson Imaging. 2007;26(6):1405–12.
78. Cihangiroglu M, Ulug AM, Firat Z, Bayram A, Kovanlikaya A, Kovanlikaya I. High b-value diffusion-weighted MR imaging of normal brain at 3T. Eur J Radiol. 2009;69(3):454–8.

79. Alvarez-Linera J, Benito-Leon J, Escribano J, Rey G. Predicting the histopathological grade of cerebral gliomas using high b value MR DW imaging at 3-tesla. J Neuroimaging. 2008;18(3):276–81.
80. Seo HS, Chang KH, Na DG, Kwon BJ, Lee DH. High b-value diffusion (b = 3000 s/mm2) MR imaging in cerebral gliomas at 3T: visual and quantitative comparisons with b = 1000 s/mm2. AJNR Am J Neuroradiol. 2008;29(3):458–63.
81. Castillo M, Smith JK, Kwock L, Wilber K. Apparent diffusion coefficients in the evaluation of high-grade cerebral gliomas. AJNR Am J Neuroradiol. 2001;22(1):60–4.
82. Mardor Y, Roth Y, Ochershvilli A, et al. Pretreatment prediction of brain tumors' response to radiation therapy using high b-value diffusion-weighted MRI. Neoplasia. 2004;6(2):136–42.
83. Yang D, Korogi Y, Sugahara T, et al. Cerebral gliomas: prospective comparison of multivoxel 2D chemical-shift imaging proton MR spectroscopy, echoplanar perfusion and diffusion-weighted MRI. Neuroradiology. 2002;44(8):656–66.
84. Barajas RF Jr, Hodgson JG, Chang JS, et al. Glioblastoma multiforme regional genetic and cellular expression patterns: influence on anatomic and physiologic MR imaging. Radiology. 2010;254(2):564–76.
85. Miloushev VZ, Chow DS, Filippi CG. Meta-analysis of diffusion metrics for the prediction of tumor grade in gliomas. AJNR Am J Neuroradiol. 2015;36(2):302–8.
86. Falk Delgado A, Nilsson M, van Westen D. Glioma grade discrimination with MR diffusion kurtosis imaging: a meta-analysis of diagnostic accuracy. Radiology. 2018;287(1):119–27.
87. Lu S, Ahn D, Johnson G, Cha S. Peritumoral diffusion tensor imaging of high-grade gliomas and metastatic brain tumors. AJNR Am J Neuroradiol. 2003;24(5):937–41.
88. Server A, Kulle B, Maehlen J, et al. Quantitative apparent diffusion coefficients in the characterization of brain tumors and associated peritumoral edema. Acta Radiol. 2009;50(6):682–9.
89. van Westen D, Latt J, Englund E, Brockstedt S, Larsson EM. Tumor extension in high-grade gliomas assessed with diffusion magnetic resonance imaging: values and lesion-to-brain ratios of apparent diffusion coefficient and fractional anisotropy. Acta Radiol. 2006;47(3):311–9.
90. Pauleit D, Langen KJ, Floeth F, et al. Can the apparent diffusion coefficient be used as a noninvasive parameter to distinguish tumor tissue from peritumoral tissue in cerebral gliomas? J Magn Reson Imaging. 2004;20(5):758–64.
91. Jiang R, Du FZ, He C, Gu M, Ke ZW, Li JH. The value of diffusion tensor imaging in differentiating high-grade gliomas from brain metastases: a systematic review and meta-analysis. PLoS One. 2014;9(11):e112550.
92. Sorensen AG, Patel S, Harmath C, et al. Comparison of diameter and perimeter methods for tumor volume calculation. J Clin Oncol. 2001;19(2):551–7.
93. Hamstra DA, Galban CJ, Meyer CR, et al. Functional diffusion map as an early imaging biomarker for high-grade glioma: correlation with conventional radiologic response and overall survival. J Clin Oncol. 2008;26(20):3387–94.
94. Tomura N, Narita K, Izumi J, et al. Diffusion changes in a tumor and peritumoral tissue after stereotactic irradiation for brain tumors: possible prediction of treatment response. J Comput Assist Tomogr. 2006;30(3):496–500.
95. Chang W, Pope WB, Harris RJ, et al. Diffusion MR characteristics following concurrent radiochemotherapy predicts progression-free and overall survival in newly diagnosed glioblastoma. Tomography. 2015;1(1):37–43.
96. Huang CF, Chou HH, Tu HT, Yang MS, Lee JK, Lin LY. Diffusion magnetic resonance imaging as an evaluation of the response of brain metastases treated by stereotactic radiosurgery. Surg Neurol. 2008;69(1):62–8; discussion 68.
97. Rock JP, Scarpace L, Hearshen D, et al. Associations among magnetic resonance spectroscopy, apparent diffusion coefficients, and image-guided histopathology with special attention to radiation necrosis. Neurosurgery. 2004;54(5):1111–7; discussion 1117–1119.
98. Al Sayyari A, Buckley R, McHenery C, Pannek K, Coulthard A, Rose S. Distinguishing recurrent primary brain tumor from radiation injury: a preliminary study using a susceptibility-weighted MR imaging-guided apparent diffusion coefficient analysis strategy. AJNR Am J Neuroradiol. 2010;31(6):1049–54.
99. Murakami R, Sugahara T, Nakamura H, et al. Malignant supratentorial astrocytoma treated with postoperative radiation therapy: prognostic value of pretreatment quantitative diffusion-weighted MR imaging. Radiology. 2007;243(2):493–9.
100. Barajas RF Jr, Rubenstein JL, Chang JS, Hwang J, Cha S. Diffusion-weighted MR imaging derived apparent diffusion coefficient is predictive of clinical outcome in primary central nervous system lymphoma. AJNR Am J Neuroradiol. 2010;31(1):60–6.
101. Ellingson BM, Rand SD, Malkin MG, Schmainda KM. Utility of functional diffusion maps to monitor a patient diagnosed with gliomatosis cerebri. J Neurooncol. 2010;97(3):419–23.
102. Brasil Caseiras G, Ciccarelli O, Altmann DR, et al. Low-grade gliomas: six-month tumor growth predicts patient outcome better than admission tumor volume, relative cerebral blood volume, and apparent diffusion coefficient. Radiology. 2009;253(2):505–12.
103. Ellingson BM, Gerstner ER, Smits M, et al. Diffusion MRI phenotypes predict overall survival benefit from anti-VEGF monotherapy in recurrent glioblastoma: converging evidence from phase II trials. Clin Cancer Res. 2017;23(19):5745–56.
104. Chakhoyan A, Woodworth DC, Harris RJ, et al. Mono-exponential, diffusion kurtosis and stretched exponential diffusion MR imaging response to chemoradiation in newly diagnosed glioblastoma. J Neurooncol. 2018;139(3):651–9.
105. Rosen BR, Belliveau JW, Vevea JM, Brady TJ. Perfusion imaging with NMR contrast agents. Magn Reson Med. 1990;14(2):249–65.
106. Belliveau JW, Rosen BR, Kantor HL, et al. Functional cerebral imaging by susceptibility-contrast NMR. Magn Reson Med. 1990;14(3):538–46.
107. Rosen BR, Belliveau JW, Aronen HJ, et al. Susceptibility contrast imaging of cerebral blood volume: human experience. Magn Reson Med. 1991;22(2):293–9; discussion 300–293.
108. Paulson ES, Schmainda KM. Comparison of dynamic susceptibility-weighted contrast-enhanced MR methods: recommendations for measuring relative cerebral blood volume in brain tumors. Radiology. 2008;249(2):601–13.
109. Boxerman JL, Bandettini PA, Kwong KK, et al. The intravascular contribution to fMRI signal change: Monte Carlo modeling and diffusion-weighted studies in vivo. Magn Reson Med. 1995;34(1):4–10.
110. Schmainda KM, Rand SD, Joseph AM, et al. Characterization of a first-pass gradient-echo spin-echo method to predict brain tumor grade and angiogenesis. AJNR Am J Neuroradiol. 2004;25(9):1524–32.
111. Donahue KM, Krouwer HG, Rand SD, et al. Utility of simultaneously acquired gradient-echo and spin-echo cerebral blood volume and morphology maps in brain tumor patients. Magn Reson Med. 2000;43(6):845–53.
112. Sugahara T, Korogi Y, Kochi M, Ushio Y, Takahashi M. Perfusion-sensitive MR imaging of gliomas: comparison between gradient-echo and spin-echo echo-planar imaging techniques. AJNR Am J Neuroradiol. 2001;22(7):1306–15.
113. Lacerda S, Law M. Magnetic resonance perfusion and permeability imaging in brain tumors. Neuroimaging Clin N Am. 2009;19(4):527–57.
114. Boxerman JL, Schmainda KM, Weisskoff RM. Relative cerebral blood volume maps corrected for contrast agent extravasation sig-

nificantly correlate with glioma tumor grade, whereas uncorrected maps do not. AJNR Am J Neuroradiol. 2006;27(4):859–67.
115. Emblem KE, Mouridsen K, Bjornerud A, et al. Vessel architectural imaging identifies cancer patient responders to anti-angiogenic therapy. Nat Med. 2013;19(9):1178–83.
116. Schmiedeskamp H, Straka M, Newbould RD, et al. Combined spin- and gradient-echo perfusion-weighted imaging. Magn Reson Med. 2012;68(1):30–40.
117. McKeown MJ, Makeig S, Brown GG, et al. Analysis of fMRI data by blind separation into independent spatial components. Hum Brain Mapp. 1998;6(3):160–88.
118. LaViolette PS, Cohen AD, Prah MA, et al. Vascular change measured with independent component analysis of dynamic susceptibility contrast MRI predicts bevacizumab response in high-grade glioma. Neuro Oncol. 2013;15(4):442–50.
119. Akbari H, Macyszyn L, Da X, et al. Pattern analysis of dynamic susceptibility contrast-enhanced MR imaging demonstrates peritumoral tissue heterogeneity. Radiology. 2014;273(2):502–10.
120. Tofts PS. Modeling tracer kinetics in dynamic Gd-DTPA MR imaging. J Magn Reson Imaging. 1997;7(1):91–101.
121. Tietze A, Mouridsen K, Mikkelsen IK. The impact of reliable prebolus T 1 measurements or a fixed T 1 value in the assessment of glioma patients with dynamic contrast enhancing MRI. Neuroradiology. 2015;57(6):561–72.
122. Haroon HA, Buckley DL, Patankar TA, et al. A comparison of Ktrans measurements obtained with conventional and first pass pharmacokinetic models in human gliomas. J Magn Reson Imaging. 2004;19(5):527–36.
123. Nam JG, Kang KM, Choi SH, et al. Comparison between the prebolus T1 measurement and the fixed T1 value in dynamic contrast-enhanced MR imaging for the differentiation of true progression from pseudoprogression in glioblastoma treated with concurrent radiation therapy and temozolomide chemotherapy. AJNR Am J Neuroradiol. 2017;38(12):2243–50.
124. Dale BM, Jesberger JA, Lewin JS, Hillenbrand CM, Duerk JL. Determining and optimizing the precision of quantitative measurements of perfusion from dynamic contrast enhanced MRI. J Magn Reson Imaging. 2003;18(5):575–84.
125. Jung SC, Yeom JA, Kim JH, et al. Glioma: application of histogram analysis of pharmacokinetic parameters from T1-weighted dynamic contrast-enhanced MR imaging to tumor grading. AJNR Am J Neuroradiol. 2014;35(6):1103–10.
126. Borogovac A, Asllani I. Arterial Spin Labeling (ASL) fMRI: advantages, theoretical constrains, and experimental challenges in neurosciences. Int J Biomed Imaging. 2012;2012:818456.
127. Deibler AR, Pollock JM, Kraft RA, Tan H, Burdette JH, Maldjian JA. Arterial spin-labeling in routine clinical practice, part 1: technique and artifacts. AJNR Am J Neuroradiol. 2008;29(7):1228–34.
128. Aronen HJ, Gazit IE, Louis DN, et al. Cerebral blood volume maps of gliomas: comparison with tumor grade and histologic findings. Radiology. 1994;191(1):41–51.
129. Aronen HJ, Perkio J. Dynamic susceptibility contrast MRI of gliomas. Neuroimaging Clin N Am. 2002;12(4):501–23.
130. Cha S, Knopp EA, Johnson G, Wetzel SG, Litt AW, Zagzag D. Intracranial mass lesions: dynamic contrast-enhanced susceptibility-weighted echo-planar perfusion MR imaging. Radiology. 2002;223(1):11–29.
131. Knopp EA, Cha S, Johnson G, et al. Glial neoplasms: dynamic contrast-enhanced T2*-weighted MR imaging. Radiology. 1999;211(3):791–8.
132. Sugahara T, Korogi Y, Kochi M, et al. Correlation of MR imaging-determined cerebral blood volume maps with histologic and angiographic determination of vascularity of gliomas. AJR Am J Roentgenol. 1998;171(6):1479–86.
133. Shin JH, Lee HK, Kwun BD, et al. Using relative cerebral blood flow and volume to evaluate the histopathologic grade of cerebral gliomas: preliminary results. AJR Am J Roentgenol. 2002;179(3):783–9.
134. Lev MH, Ozsunar Y, Henson JW, et al. Glial tumor grading and outcome prediction using dynamic spin-echo MR susceptibility mapping compared with conventional contrast-enhanced MR: confounding effect of elevated rCBV of oligodendrogliomas [corrected]. AJNR Am J Neuroradiol. 2004;25(2):214–21.
135. Chawla S, Wang S, Wolf RL, et al. Arterial spin-labeling and MR spectroscopy in the differentiation of gliomas. AJNR Am J Neuroradiol. 2007;28(9):1683–9.
136. Chawla A, Emmanuel JV, Seow WT, Lou J, Teo HE, Lim CC. Paediatric PNET: pre-surgical MRI features. Clin Radiol. 2007;62(1):43–52.
137. Hartmann M, Heiland S, Harting I, et al. Distinguishing of primary cerebral lymphoma from high-grade glioma with perfusion-weighted magnetic resonance imaging. Neurosci Lett. 2003;338(2):119–22.
138. Jia Z, Geng D, Xie T, Zhang J, Liu Y. Quantitative analysis of neovascular permeability in glioma by dynamic contrast-enhanced MR imaging. J Clin Neurosci. 2012;19(6):820–3.
139. Mills SJ, du Plessis D, Pal P, et al. Mitotic activity in glioblastoma correlates with estimated extravascular extracellular space derived from dynamic contrast-enhanced MR imaging. AJNR Am J Neuroradiol. 2016;37(5):811–7.
140. Wolf RL, Wang J, Wang S, et al. Grading of CNS neoplasms using continuous arterial spin labeled perfusion MR imaging at 3 Tesla. J Magn Reson Imaging. 2005;22(4):475–82.
141. Noguchi T, Yoshiura T, Hiwatashi A, et al. Perfusion imaging of brain tumors using arterial spin-labeling: correlation with histopathologic vascular density. AJNR Am J Neuroradiol. 2008;29(4):688–93.
142. Arisawa A, Watanabe Y, Tanaka H, et al. Comparative study of pulsed-continuous arterial spin labeling and dynamic susceptibility contrast imaging by histogram analysis in evaluation of glial tumors. Neuroradiology. 2018;60(6):599–608.
143. Falk Delgado A, De Luca F, van Westen D. Arterial spin labeling MR imaging for differentiation between high- and low-grade glioma-a meta-analysis. Neuro Oncol. 2018;20(11):1450–61.
144. Martin AJ, Liu H, Hall WA, Truwit CL. Preliminary assessment of turbo spectroscopic imaging for targeting in brain biopsy. AJNR Am J Neuroradiol. 2001;22(5):959–68.
145. Danchaivijitr N, Waldman AD, Tozer DJ, et al. Low-grade gliomas: do changes in rCBV measurements at longitudinal perfusion-weighted MR imaging predict malignant transformation? Radiology. 2008;247(1):170–8.
146. Law M, Young RJ, Babb JS, et al. Gliomas: predicting time to progression or survival with cerebral blood volume measurements at dynamic susceptibility-weighted contrast-enhanced perfusion MR imaging. Radiology. 2008;247(2):490–8.
147. Choi YS, Kim DW, Lee SK, et al. The added prognostic value of preoperative dynamic contrast-enhanced MRI histogram analysis in patients with glioblastoma: analysis of overall and progression-free survival. AJNR Am J Neuroradiol. 2015;36(12):2235–41.
148. Furtner J, Bender B, Braun C, et al. Prognostic value of blood flow measurements using arterial spin labeling in gliomas. PLoS One. 2014;9(6):e99616.
149. Rau MK, Braun C, Skardelly M, et al. Prognostic value of blood flow estimated by arterial spin labeling and dynamic susceptibility contrast-enhanced MR imaging in high-grade gliomas. J Neurooncol. 2014;120(3):557–66.
150. Kickingereder P, Wiestler B, Burth S, et al. Relative cerebral blood volume is a potential predictive imaging biomarker of bevacizumab efficacy in recurrent glioblastoma. Neuro Oncol. 2015;17(8):1139–47.
151. Schmainda KM, Prah M, Connelly J, et al. Dynamic-susceptibility contrast agent MRI measures of relative cerebral blood volume

predict response to bevacizumab in recurrent high-grade glioma. Neuro Oncol. 2014;16(6):880–8.
152. Verhoeff JJ, Lavini C, van Linde ME, et al. Bevacizumab and dose-intense temozolomide in recurrent high-grade glioma. Ann Oncol. 2010;21(8):1723–7.
153. Mangla R, Singh G, Ziegelitz D, et al. Changes in relative cerebral blood volume 1 month after radiation-temozolomide therapy can help predict overall survival in patients with glioblastoma. Radiology. 2010;256(2):575–84.
154. Galban CJ, Chenevert TL, Meyer CR, et al. The parametric response map is an imaging biomarker for early cancer treatment outcome. Nat Med. 2009;15(5):572–6.
155. Lemasson B, Chenevert TL, Lawrence TS, et al. Impact of perfusion map analysis on early survival prediction accuracy in glioma patients. Transl Oncol. 2013;6(6):766–74.
156. Schmainda KM, Zhang Z, Prah M, et al. Dynamic susceptibility contrast MRI measures of relative cerebral blood volume as a prognostic marker for overall survival in recurrent glioblastoma: results from the ACRIN 6677/RTOG 0625 multicenter trial. Neuro Oncol. 2015;17(8):1148–56.
157. Choi SH, Jung SC, Kim KW, et al. Perfusion MRI as the predictive/prognostic and pharmacodynamic biomarkers in recurrent malignant glioma treated with bevacizumab: a systematic review and a time-to-event meta-analysis. J Neurooncol. 2016;128(2):185–94.
158. Young GS. Advanced MRI of adult brain tumors. Neurol Clin. 2007;25(4):947–73, viii.
159. Cha S. Neuroimaging in neuro-oncology. Neurotherapeutics. 2009;6(3):465–77.
160. Hakyemez B, Erdogan C, Bolca N, Yildirim N, Gokalp G, Parlak M. Evaluation of different cerebral mass lesions by perfusion-weighted MR imaging. J Magn Reson Imaging. 2006;24(4):817–24.
161. Brunberg JA, Chenevert TL, McKeever PE, et al. In vivo MR determination of water diffusion coefficients and diffusion anisotropy: correlation with structural alteration in gliomas of the cerebral hemispheres. AJNR Am J Neuroradiol. 1995;16(2):361–71.
162. Chinn RJ, Wilkinson ID, Hall-Craggs MA, et al. Toxoplasmosis and primary central nervous system lymphoma in HIV infection: diagnosis with MR spectroscopy. Radiology. 1995;197(3):649–54.
163. Ernst TM, Chang L, Witt MD, et al. Cerebral toxoplasmosis and lymphoma in AIDS: perfusion MR imaging experience in 13 patients. Radiology. 1998;208(3):663–9.
164. Mangla R, Kolar B, Zhu T, Zhong J, Almast J, Ekholm S. Percentage signal recovery derived from MR dynamic susceptibility contrast imaging is useful to differentiate common enhancing malignant lesions of the brain. AJNR Am J Neuroradiol. 2011;32(6):1004–10.
165. Xing Z, You RX, Li J, Liu Y, Cao DR. Differentiation of primary central nervous system lymphomas from high-grade gliomas by rCBV and percentage of signal intensity recovery derived from dynamic susceptibility-weighted contrast-enhanced perfusion MR imaging. Clin Neuroradiol. 2014;24(4):329–36.
166. Kickingereder P, Wiestler B, Sahm F, et al. Primary central nervous system lymphoma and atypical glioblastoma: multiparametric differentiation by using diffusion-, perfusion-, and susceptibility-weighted MR imaging. Radiology. 2014;272(3):843–50.
167. Lu S, Wang S, Gao Q, et al. Quantitative evaluation of diffusion and dynamic contrast-enhanced magnetic resonance imaging for differentiation between primary central nervous system lymphoma and glioblastoma. J Comput Assist Tomogr. 2017;41(6):898–903.
168. Howe FA, Barton SJ, Cudlip SA, et al. Metabolic profiles of human brain tumors using quantitative in vivo 1H magnetic resonance spectroscopy. Magn Reson Med. 2003;49(2):223–32.
169. Burtscher IM, Stahlberg F, Holtas S. Proton (1H) MR spectroscopy for routine diagnostic evaluation of brain lesions. Acta Radiol. 1997;38(6):953–60.
170. Hayashida Y, Hirai T, Morishita S, et al. Diffusion-weighted imaging of metastatic brain tumors: comparison with histologic type and tumor cellularity. AJNR Am J Neuroradiol. 2006;27(7):1419–25.
171. Cha S, Lupo JM, Chen MH, et al. Differentiation of glioblastoma multiforme and single brain metastasis by peak height and percentage of signal intensity recovery derived from dynamic susceptibility-weighted contrast-enhanced perfusion MR imaging. AJNR Am J Neuroradiol. 2007;28(6):1078–84.
172. Bitsch A, Bruhn H, Vougioukas V, et al. Inflammatory CNS demyelination: histopathologic correlation with in vivo quantitative proton MR spectroscopy. AJNR Am J Neuroradiol. 1999;20(9):1619–27.
173. Saindane AM, Cha S, Law M, Xue X, Knopp EA, Zagzag D. Proton MR spectroscopy of tumefactive demyelinating lesions. AJNR Am J Neuroradiol. 2002;23(8):1378–86.
174. Bernarding J, Braun J, Koennecke HC. Diffusion- and perfusion-weighted MR imaging in a patient with acute demyelinating encephalomyelitis (ADEM). J Magn Reson Imaging. 2002;15(1):96–100.
175. Sener RN. Rasmussen's encephalitis: proton MR spectroscopy and diffusion MR findings. J Neuroradiol. 2000;27(3):179–84.
176. Bulakbasi N, Kocaoglu M. Central nervous system infections of herpesvirus family. Neuroimaging Clin N Am. 2008;18(1):53–84, viii.
177. Tyrakowska-Dadello Z, Tarasow E, Janusek D, Moniuszko-Malinowska A, Zajkowska J, Pancewicz S. Brain perfusion alterations in tick-borne encephalitis-preliminary report. Int J Infect Dis. 2018;68:26–30.
178. Pal D, Bhattacharyya A, Husain M, Prasad KN, Pandey CM, Gupta RK. In vivo proton MR spectroscopy evaluation of pyogenic brain abscesses: a report of 194 cases. AJNR Am J Neuroradiol. 2010;31(2):360–6.
179. Luthra G, Parihar A, Nath K, et al. Comparative evaluation of fungal, tubercular, and pyogenic brain abscesses with conventional and diffusion MR imaging and proton MR spectroscopy. AJNR Am J Neuroradiol. 2007;28(7):1332–8.
180. Xu XX, Li B, Yang HF, et al. Can diffusion-weighted imaging be used to differentiate brain abscess from other ring-enhancing brain lesions? A meta-analysis. Clin Radiol. 2014;69(9):909–15.
181. Chan JH, Tsui EY, Chau LF, et al. Discrimination of an infected brain tumor from a cerebral abscess by combined MR perfusion and diffusion imaging. Comput Med Imaging Graph. 2002;26(1):19–23.
182. Floriano VH, Torres US, Spotti AR, Ferraz-Filho JR, Tognola WA. The role of dynamic susceptibility contrast-enhanced perfusion MR imaging in differentiating between infectious and neoplastic focal brain lesions: results from a cohort of 100 consecutive patients. PLoS One. 2013;8(12):e81509.
183. Chawla S, Wang S, Mohan S, et al. Differentiation of brain infection from necrotic glioblastoma using combined analysis of diffusion and perfusion MRI. J Magn Reson Imaging. 2019;49(1):184–94.
184. White ML, Zhang Y, Kirby P, Ryken TC. Can tumor contrast enhancement be used as a criterion for differentiating tumor grades of oligodendrogliomas? AJNR Am J Neuroradiol. 2005;26(4):784–90.
185. Spampinato MV, Smith JK, Kwock L, et al. Cerebral blood volume measurements and proton MR spectroscopy in grading of oligodendroglial tumors. AJR Am J Roentgenol. 2007;188(1):204–12.
186. Camacho DL, Smith JK, Grimme JD, Keyserling HF, Castillo M. Atypical MR imaging perfusion in developmental venous anomalies. AJNR Am J Neuroradiol. 2004;25(9):1549–52.
187. Ball WS Jr, Holland SK. Perfusion imaging in the pediatric patient. Magn Reson Imaging Clin N Am. 2001;9(1):207–30, ix.

188. Wang Z, Sutton LN, Cnaan A, et al. Proton MR spectroscopy of pediatric cerebellar tumors. AJNR Am J Neuroradiol. 1995;16(9):1821–33.
189. Kovanlikaya A, Panigrahy A, Krieger MD, et al. Untreated pediatric primitive neuroectodermal tumor in vivo: quantitation of taurine with MR spectroscopy. Radiology. 2005;236(3):1020–5.
190. Rumboldt Z, Camacho DL, Lake D, Welsh CT, Castillo M. Apparent diffusion coefficients for differentiation of cerebellar tumors in children. AJNR Am J Neuroradiol. 2006;27(6):1362–9.
191. Gauvain KM, McKinstry RC, Mukherjee P, et al. Evaluating pediatric brain tumor cellularity with diffusion-tensor imaging. AJR Am J Roentgenol. 2001;177(2):449–54.
192. Girard N, Wang ZJ, Erbetta A, et al. Prognostic value of proton MR spectroscopy of cerebral hemisphere tumors in children. Neuroradiology. 1998;40(2):121–5.
193. Warren KE, Frank JA, Black JL, et al. Proton magnetic resonance spectroscopic imaging in children with recurrent primary brain tumors. J Clin Oncol. 2000;18(5):1020–6.
194. Dangouloff-Ros V, Deroulers C, Foissac F, et al. Arterial spin labeling to predict brain tumor grading in children: correlations between histopathologic vascular density and perfusion MR imaging. Radiology. 2016;281(2):553–66.
195. Valk PE, Dillon WP. Radiation injury of the brain. AJNR Am J Neuroradiol. 1991;12(1):45–62.
196. Schiffer D, Giordana MT, Soffietti R, Sciolla R. Histological observations on the regrowth of malignant gliomas after radiotherapy and chemotherapy. Acta Neuropathol. 1982;58(4):291–9.
197. Stupp R, Mason WP, van den Bent MJ, et al. Radiotherapy plus concomitant and adjuvant temozolomide for glioblastoma. N Engl J Med. 2005;352(10):987–96.
198. Giglio P, Gilbert MR. Cerebral radiation necrosis. Neurologist. 2003;9(4):180–8.
199. Kumar AJ, Leeds NE, Fuller GN, et al. Malignant gliomas: MR imaging spectrum of radiation therapy- and chemotherapy-induced necrosis of the brain after treatment. Radiology. 2000;217(2):377–84.
200. Dalesandro MF, Andre JB. Posttreatment evaluation of brain gliomas. Neuroimaging Clin N Am. 2016;26(4):581–99.
201. Kruser TJ, Mehta MP, Robins HI. Pseudoprogression after glioma therapy: a comprehensive review. Expert Rev Neurother. 2013;13(4):389–403.
202. Gunjur A, Lau E, Taouk Y, Ryan G. Early post-treatment pseudoprogression amongst glioblastoma multiforme patients treated with radiotherapy and temozolomide: a retrospective analysis. J Med Imaging Radiat Oncol. 2011;55(6):603–10.
203. Roldan GB, Scott JN, McIntyre JB, et al. Population-based study of pseudoprogression after chemoradiotherapy in GBM. Can J Neurol Sci. 2009;36(5):617–22.
204. Brandes AA, Franceschi E, Tosoni A, et al. MGMT promoter methylation status can predict the incidence and outcome of pseudoprogression after concomitant radiochemotherapy in newly diagnosed glioblastoma patients. J Clin Oncol. 2008;26(13):2192–7.
205. Sugahara T, Korogi Y, Tomiguchi S, et al. Posttherapeutic intraaxial brain tumor: the value of perfusion-sensitive contrast-enhanced MR imaging for differentiating tumor recurrence from nonneoplastic contrast-enhancing tissue. AJNR Am J Neuroradiol. 2000;21(5):901–9.
206. Hu LS, Baxter LC, Smith KA, et al. Relative cerebral blood volume values to differentiate high-grade glioma recurrence from posttreatment radiation effect: direct correlation between image-guided tissue histopathology and localized dynamic susceptibility-weighted contrast-enhanced perfusion MR imaging measurements. AJNR Am J Neuroradiol. 2009;30(3):552–8.
207. Wang S, Martinez-Lage M, Sakai Y, et al. Differentiating tumor progression from pseudoprogression in patients with glioblastomas using diffusion tensor imaging and dynamic susceptibility contrast MRI. AJNR Am J Neuroradiol. 2016;37(1):28–36.
208. Boxerman JL, Ellingson BM, Jeyapalan S, et al. Longitudinal DSC-MRI for distinguishing tumor recurrence from pseudoprogression in patients with a high-grade glioma. Am J Clin Oncol. 2017;40(3):228–34.
209. Hu X, Wong KK, Young GS, Guo L, Wong ST. Support vector machine multiparametric MRI identification of pseudoprogression from tumor recurrence in patients with resected glioblastoma. J Magn Reson Imaging. 2011;33(2):296–305.
210. Thomas AA, Arevalo-Perez J, Kaley T, et al. Dynamic contrast enhanced T1 MRI perfusion differentiates pseudoprogression from recurrent glioblastoma. J Neurooncol. 2015;125(1):183–90.
211. Yun TJ, Park CK, Kim TM, et al. Glioblastoma treated with concurrent radiation therapy and temozolomide chemotherapy: differentiation of true progression from pseudoprogression with quantitative dynamic contrast-enhanced MR imaging. Radiology. 2015;274(3):830–40.
212. Nabavizadeh SA. Quantitative dynamic contrast-enhanced MR imaging in posttreatment glioblastoma: possible limitations of short acquisition time. Radiology. 2016;279(1):326.
213. Bisdas S, Naegele T, Ritz R, et al. Distinguishing recurrent high-grade gliomas from radiation injury: a pilot study using dynamic contrast-enhanced MR imaging. Acad Radiol. 2011;18(5):575–83.
214. Chung WJ, Kim HS, Kim N, Choi CG, Kim SJ. Recurrent glioblastoma: optimum area under the curve method derived from dynamic contrast-enhanced T1-weighted perfusion MR imaging. Radiology. 2013;269(2):561–8.
215. Nyberg E, Honce J, Kleinschmidt-DeMasters BK, Shukri B, Kreidler S, Nagae L. Arterial spin labeling: pathologically proven superiority over conventional MRI for detection of high-grade glioma progression after treatment. Neuroradiol J. 2016;29(5):377–83.
216. Ye J, Bhagat SK, Li H, et al. Differentiation between recurrent gliomas and radiation necrosis using arterial spin labeling perfusion imaging. Exp Ther Med. 2016;11(6):2432–6.
217. Choi YJ, Kim HS, Jahng GH, Kim SJ, Suh DC. Pseudoprogression in patients with glioblastoma: added value of arterial spin labeling to dynamic susceptibility contrast perfusion MR imaging. Acta Radiol. 2013;54(4):448–54.
218. Razek A, El-Serougy L, Abdelsalam M, Gaballa G, Talaat M. Differentiation of residual/recurrent gliomas from postradiation necrosis with arterial spin labeling and diffusion tensor magnetic resonance imaging-derived metrics. Neuroradiology. 2018;60(2):169–77.
219. Hein PA, Eskey CJ, Dunn JF, Hug EB. Diffusion-weighted imaging in the follow-up of treated high-grade gliomas: tumor recurrence versus radiation injury. AJNR Am J Neuroradiol. 2004;25(2):201–9.
220. Rabinov JD, Lee PL, Barker FG, et al. In vivo 3-T MR spectroscopy in the distinction of recurrent glioma versus radiation effects: initial experience. Radiology. 2002;225(3):871–9.
221. Bobek-Billewicz B, Stasik-Pres G, Majchrzak H, Zarudzki L. Differentiation between brain tumor recurrence and radiation injury using perfusion, diffusion-weighted imaging and MR spectroscopy. Folia Neuropathol. 2010;48(2):81–92.
222. Zeng QS, Li CF, Liu H, Zhen JH, Feng DC. Distinction between recurrent glioma and radiation injury using magnetic resonance spectroscopy in combination with diffusion-weighted imaging. Int J Radiat Oncol Biol Phys. 2007;68(1):151–8.
223. Cha J, Kim ST, Kim HJ, et al. Differentiation of tumor progression from pseudoprogression in patients with posttreatment glioblastoma using multiparametric histogram analysis. AJNR Am J Neuroradiol. 2014;35(7):1309–17.

224. Brandsma D, van den Bent MJ. Pseudoprogression and pseudoresponse in the treatment of gliomas. Curr Opin Neurol. 2009;22(6):633–8.
225. Clarke JL, Chang S. Pseudoprogression and pseudoresponse: challenges in brain tumor imaging. Curr Neurol Neurosci Rep. 2009;9(3):241–6.
226. de Groot JF, Yung WK. Bevacizumab and irinotecan in the treatment of recurrent malignant gliomas. Cancer J. 2008;14(5):279–85.
227. Rauscher A, Sedlacik J, Barth M, Haacke EM, Reichenbach JR. Noninvasive assessment of vascular architecture and function during modulated blood oxygenation using susceptibility weighted magnetic resonance imaging. Magn Reson Med. 2005;54(1):87–95.
228. Cao Y, Tsien CI, Nagesh V, et al. Survival prediction in high-grade gliomas by MRI perfusion before and during early stage of RT. Int J Radiat Oncol Biol Phys. 2006;64(3):876–85.
229. Kapoor GS, Gocke TA, Chawla S, et al. Magnetic resonance perfusion-weighted imaging defines angiogenic subtypes of oligodendroglioma according to 1p19q and EGFR status. J Neurooncol. 2009;92(3):373–86.
230. Batchelor TT, Sorensen AG, di Tomaso E, et al. AZD2171, a pan-VEGF receptor tyrosine kinase inhibitor, normalizes tumor vasculature and alleviates edema in glioblastoma patients. Cancer Cell. 2007;11(1):83–95.
231. Zacharaki EI, Shen D, Lee SK, Davatzikos C. ORBIT: a multiresolution framework for deformable registration of brain tumor images. IEEE Trans Med Imaging. 2008;27(8):1003–17.
232. Verma R, Zacharaki EI, Ou Y, et al. Multiparametric tissue characterization of brain neoplasms and their recurrence using pattern classification of MR images. Acad Radiol. 2008;15(8):966–77.
233. Shrot S, Salhov M, Dvorski N, Konen E, Averbuch A, Hoffmann C. Application of MR morphologic, diffusion tensor, and perfusion imaging in the classification of brain tumors using machine learning scheme. Neuroradiology. 2019;61(7):757–65.
234. Rudie JD, Rauschecker AM, Bryan RN, Davatzikos C, Mohan S. Emerging applications of artificial intelligence in neuro-oncology. Radiology. 2019;290(3):607–18.
235. Goldmacher GV, Ellingson BM, Boxerman J, Barboriak D, Pope WB, Gilbert M. Standardized brain tumor imaging protocol for clinical trials. AJNR Am J Neuroradiol. 2015;36(10):E65–6.
236. Ellingson BM, Bendszus M, Boxerman J, et al. Consensus recommendations for a standardized brain tumor imaging protocol in clinical trials. Neuro Oncol. 2015;17(9):1188–98.
237. Schmainda KM, Prah MA, Hu LS, et al. Moving toward a consensus DSC-MRI protocol: validation of a low-flip angle single-dose option as a reference standard for brain tumors. AJNR Am J Neuroradiol. 2019;40(4):626–33.
238. Hollingworth W, Medina LS, Lenkinski RE, et al. A systematic literature review of magnetic resonance spectroscopy for the characterization of brain tumors. AJNR Am J Neuroradiol. 2006;27(7):1404–11.